ChE 430
Nanomaterials for Chemical Engineering Applications

MODULE 9: PHOTO-ELECTROCHEMICAL AND PHOTO-CATALYTIC CELLS

9.0. Introduction and motivation
9.1. Panel-type cell
9.2. Particle-based reactors
9.3. New concepts using nanomaterials

9.0. Introduction and motivation

Plants use CO_2 and the energy from the sun to make sugars, which are high energy dense molecules

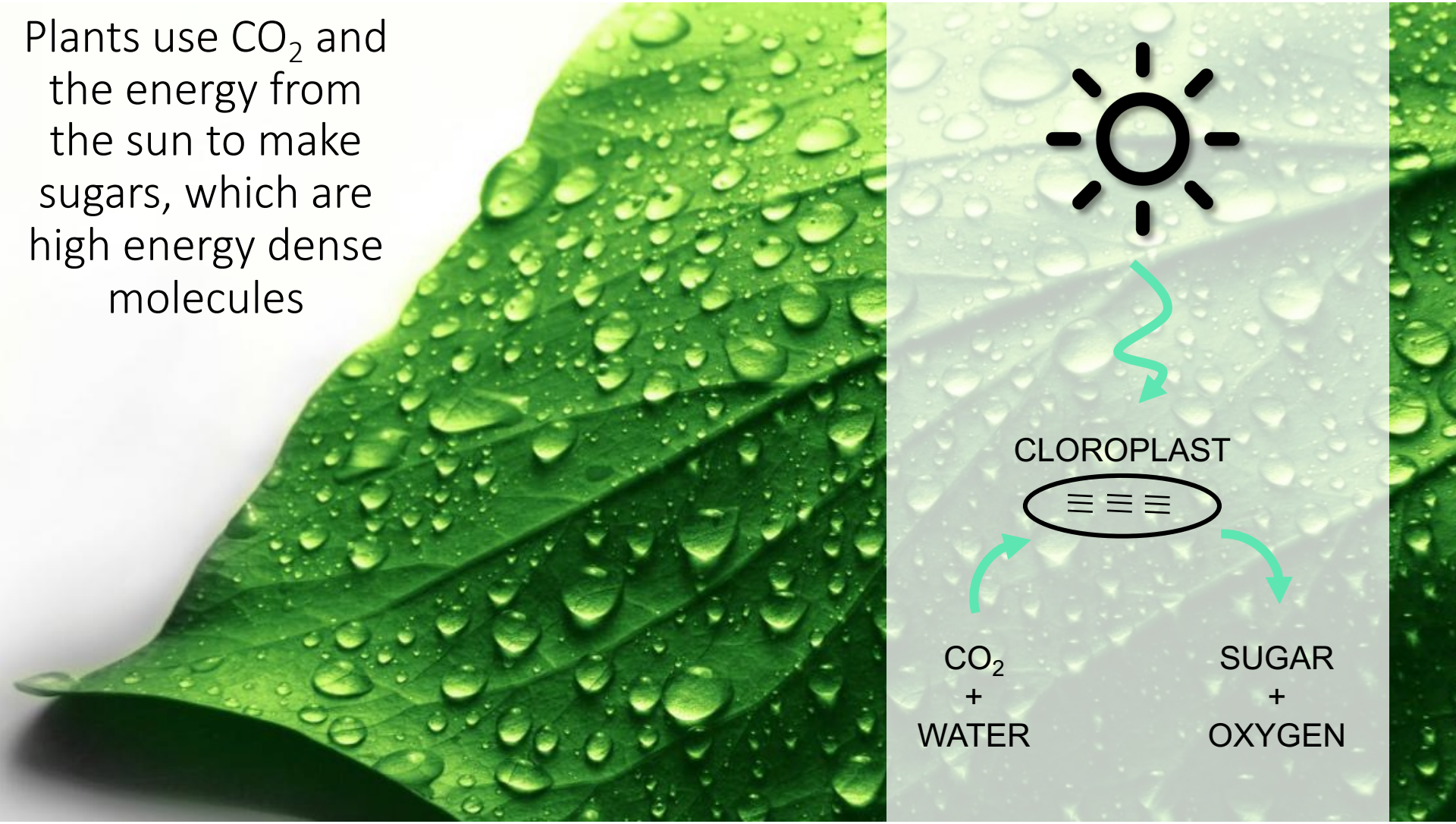

9.0. Introduction and motivation

Can we build artificial systems that store energy into useful chemicals?

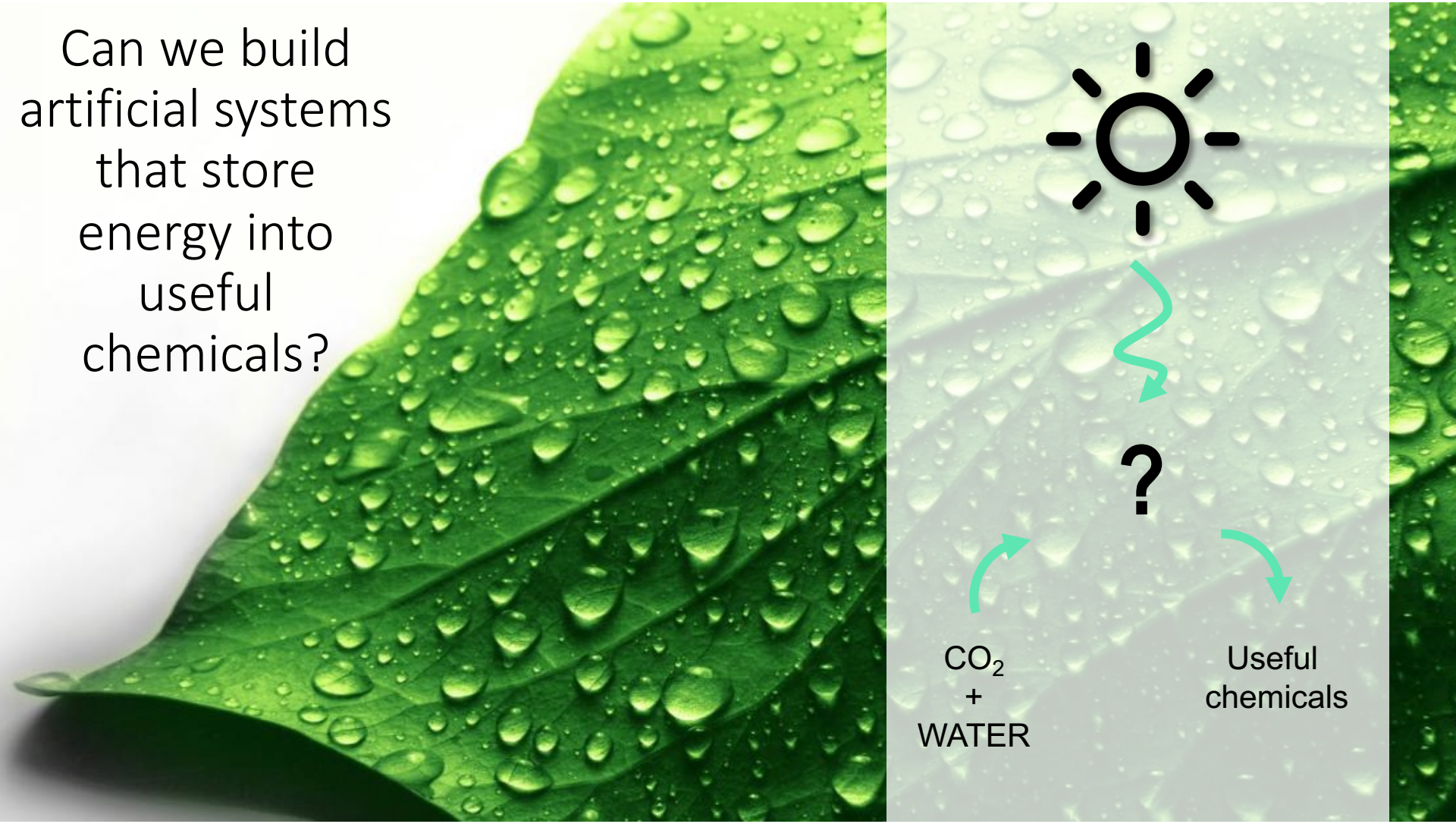

9.0. Introduction and motivation

PV + Electrolysis

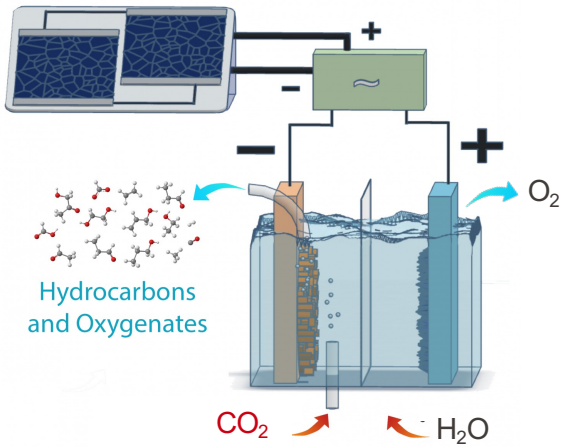

Solar-to-hydrogen: up to 30%

Photoelectrochemistry

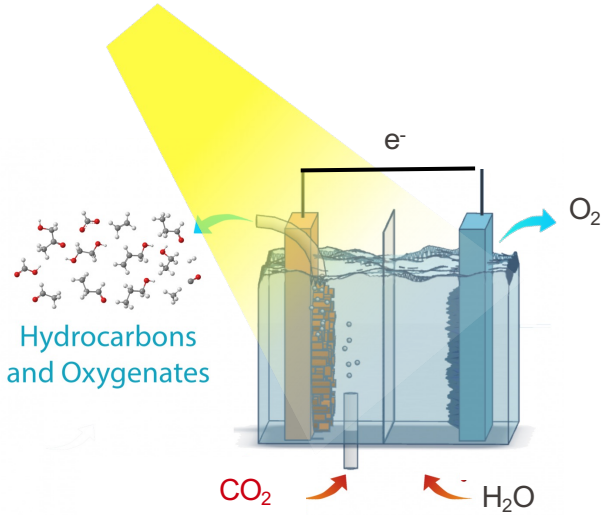

Solar-to-hydrogen: up to 16%

Photocatalysis

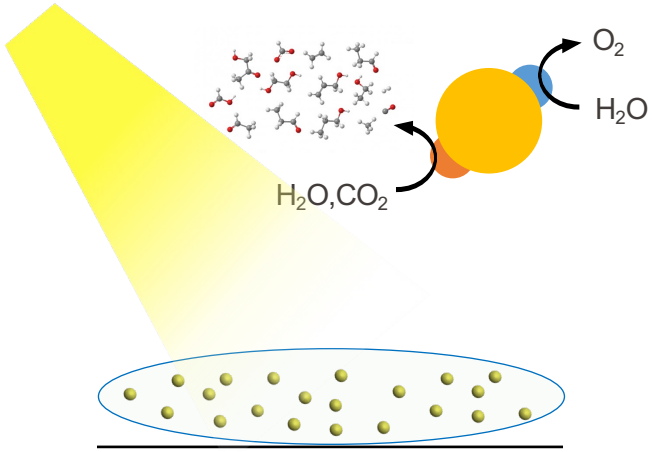

Solar-to-hydrogen: 1-6%

Ager et al. Energy Environ. Sci. (**2015**); Jaramillo et al. Nat. Commun. (**2016**); Turner, TG Deutsch Nat. Energy. (**2017**)

9.0. Introduction and motivation

Honda and Fujishima (Nature 1972)

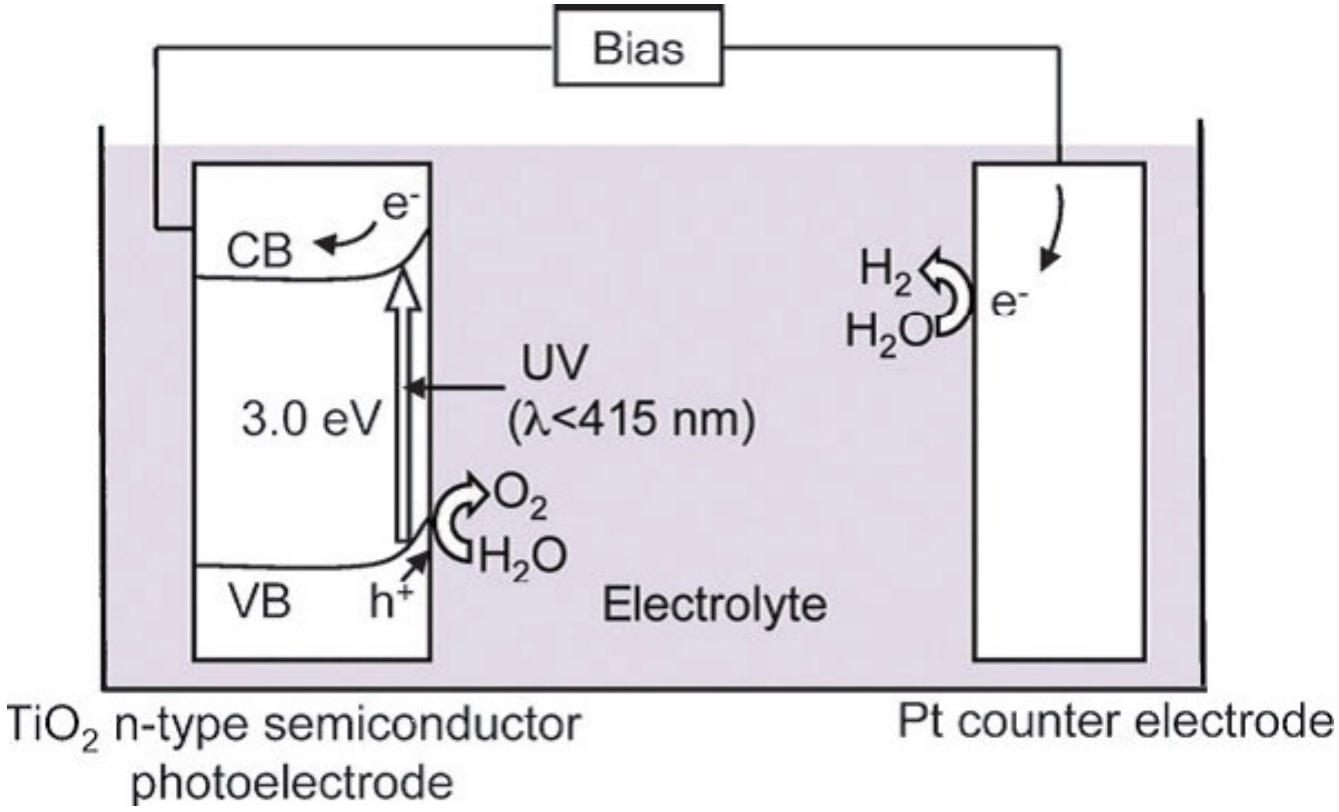

9.0. Introduction and motivation

If we want to use one single light absorber

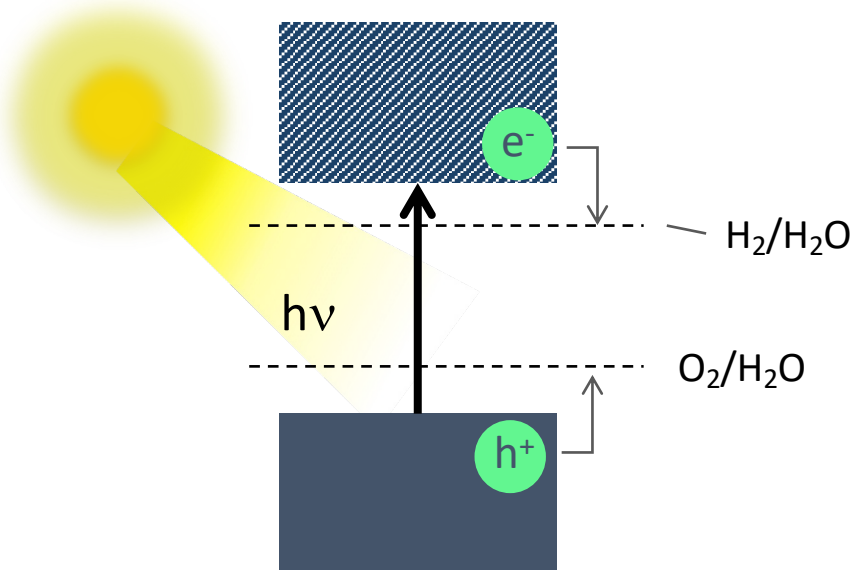

Ideal semiconductors to convert photons into highly reducing electrons and highly oxidative holes:

- Band gap (1.7-2eV)
- Efficient charge generation and separation
- Band edge position
- Photocorrosion

9.0. Introduction and motivation

Two is better than one!

For a single light absorber

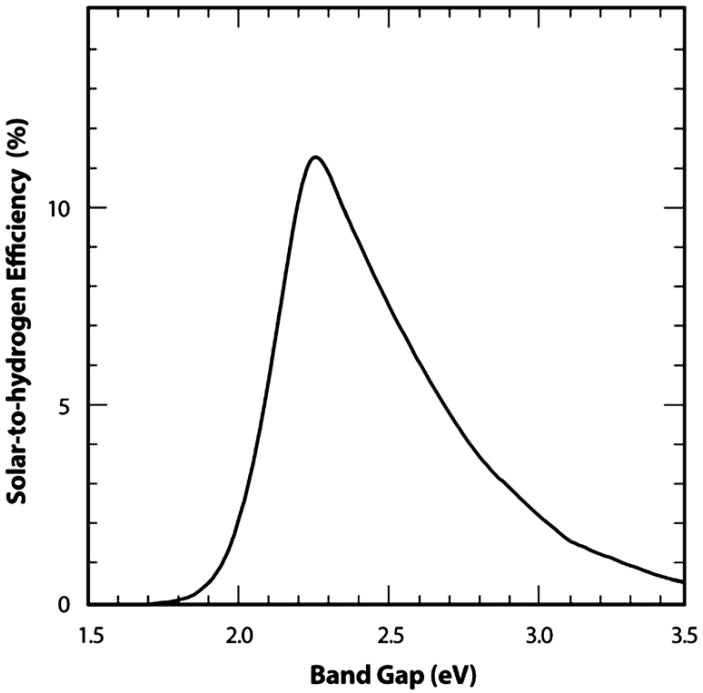

In a tandem configuration

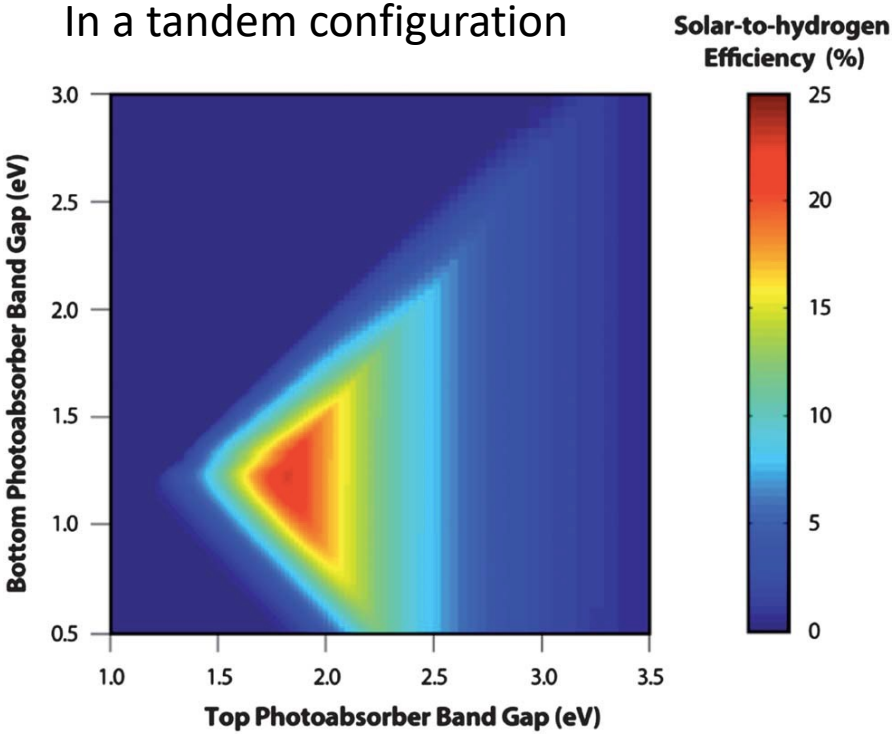

Pinaud et al. Energy Environ. Sci. 2013, 6, 1983

Solar-to-hydrogen (STH) refers to how many of the incident illumination power density is converted into hydrogen

9.0. Introduction and motivation

What about matching with the catalyst?

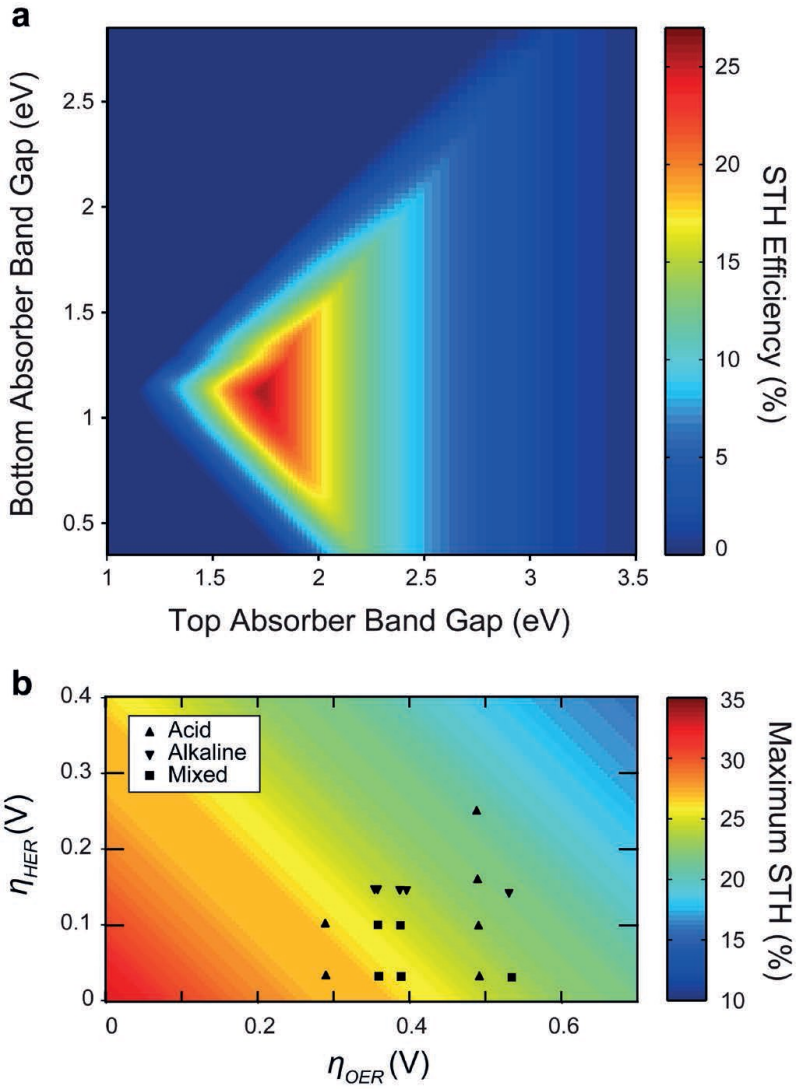

Figure 2 | STH efficiency contour plots as a function of bandgaps and electrocatalytic overpotentials for the top and bottom absorbers of a dual (stacked) absorber PEC water splitting device. **a**, Calculated STH efficiencies are modelled using some of the most active catalysts for the HER (Pt) and the OER ($NiFeO_x$), and free energy losses equalling approximately 15–30% of the total bandgap of each semiconductor absorber. **b**, Dependence of the maximum achievable STH efficiency as a function of overpotential for the hydrogen evolution reaction (η_{HER}) and the oxygen evolution reaction (η_{OER}), based on published catalyst activities using geometric area normalized current densities, with data points showing potential devices for acid only, alkaline only, or mixed systems[29–39].

Montoya et al. Nature Mater Review (2016)

9.0. Introduction and motivation

The stability issue in light absorbers

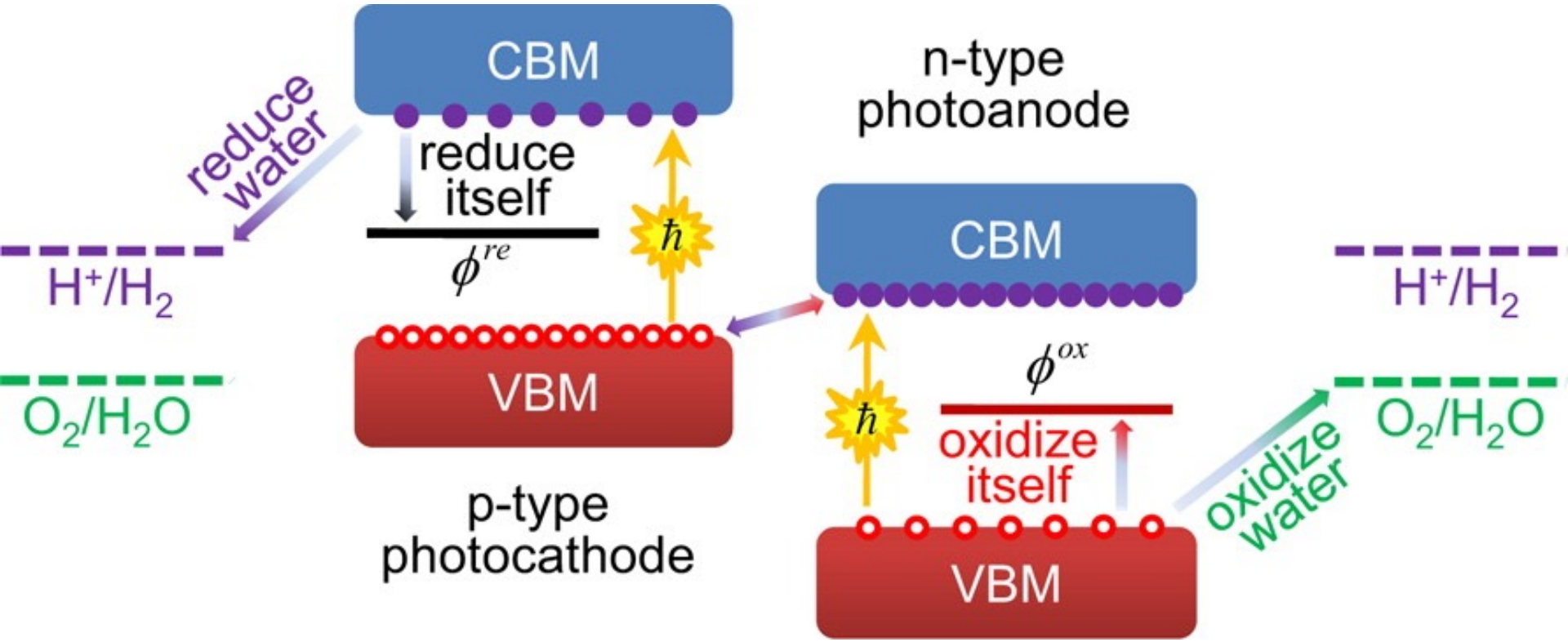

Lin Wang Wang, Chemistry of Materials 2012, 24, 3659

9.0. Introduction and motivation

The stability issue in light absorbers

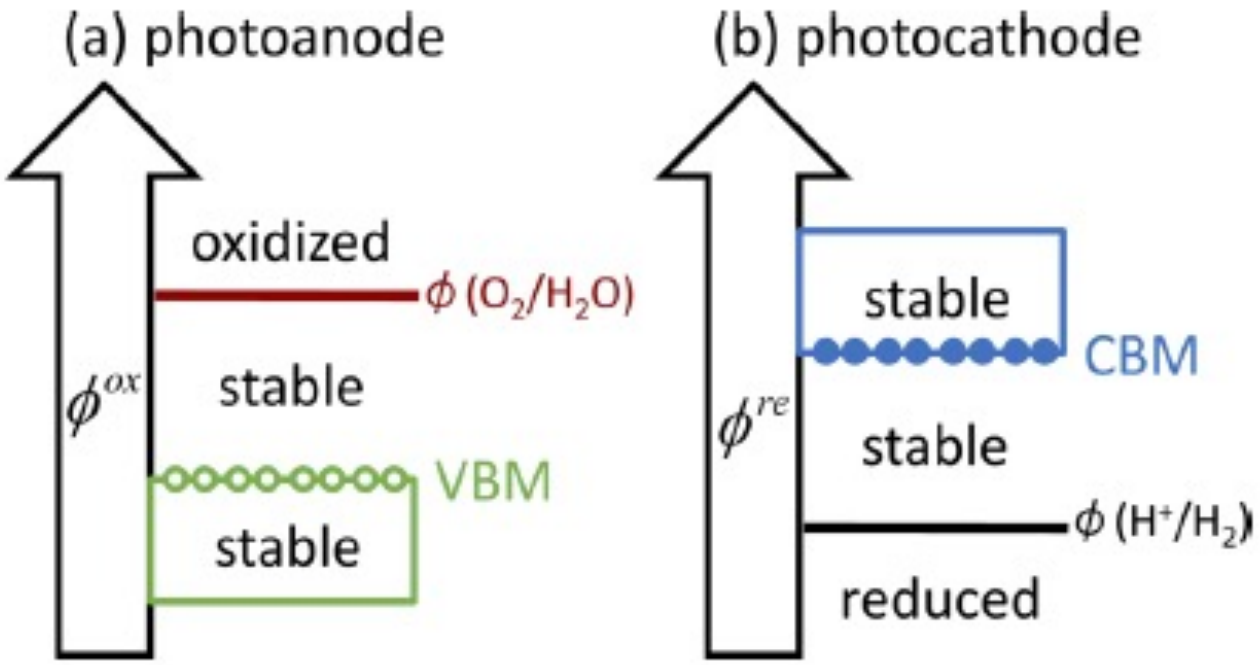

Figure 2. Stability change of the photoanode (a) as its oxidation potential ϕ^{ox} shifts up from below the VBM to above $\phi(O_2/H_2O)$ and of the photocathode (b) as its reduction potential ϕ^{re} shifts down from above the CBM to below $\phi(H^+/H_2)$.

9.0. Introduction and motivation

How to think about photocorrosion

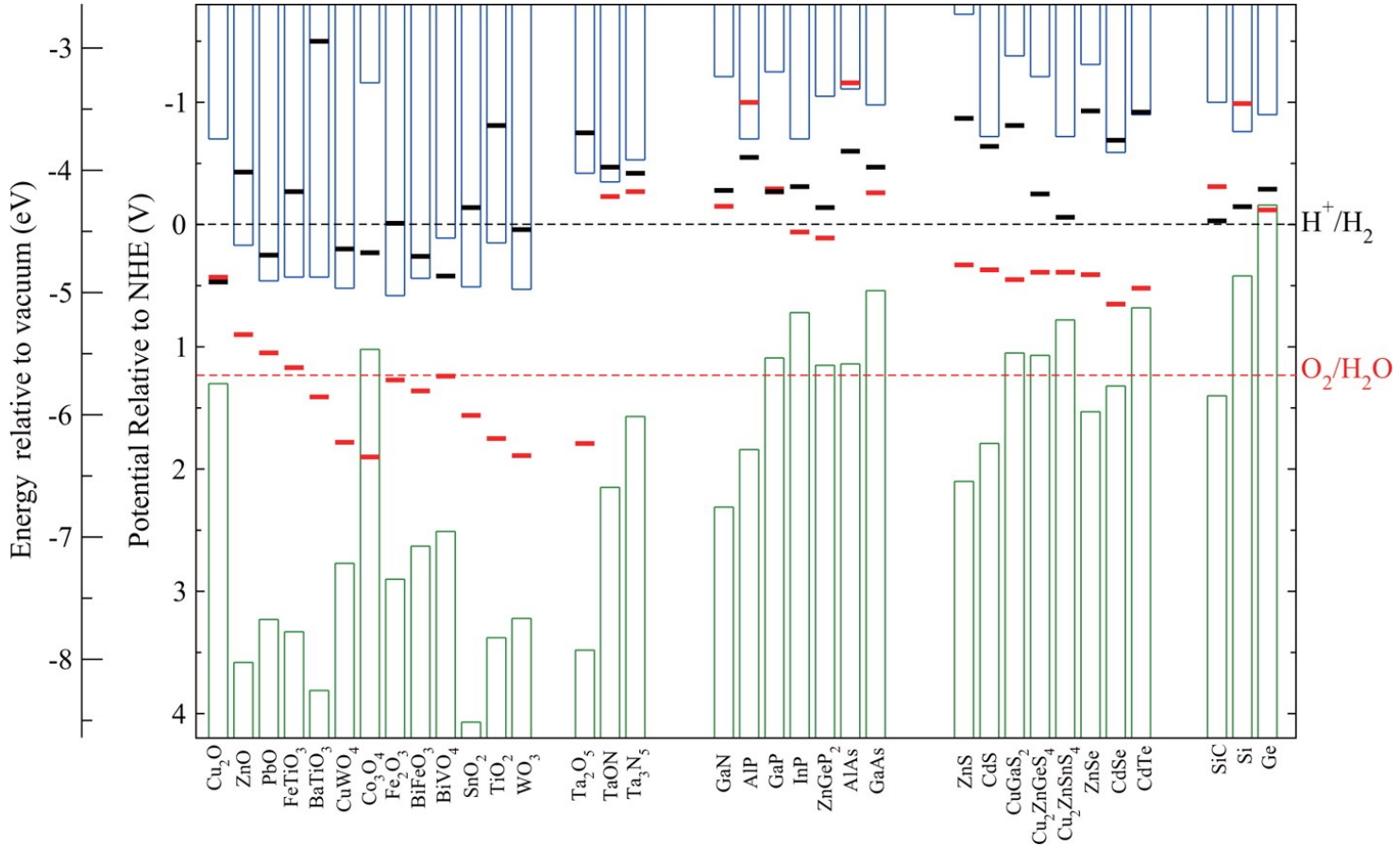

Calculated oxidation potential ϕ^{ox} (**red bars**) and reduction potential ϕ^{re} (**black bars**) relative to the NHE and vacuum level for a series of semiconductors in solution at pH = 0, the ambient temperature 298.15 K, and pressure 1 bar.

9.1. Panel-type CELLS

Protected Major Semiconductor Classes:

- Group IV, III-V, II-VI; MOx
- Planar, nanostructured, poly- and single-crystalline

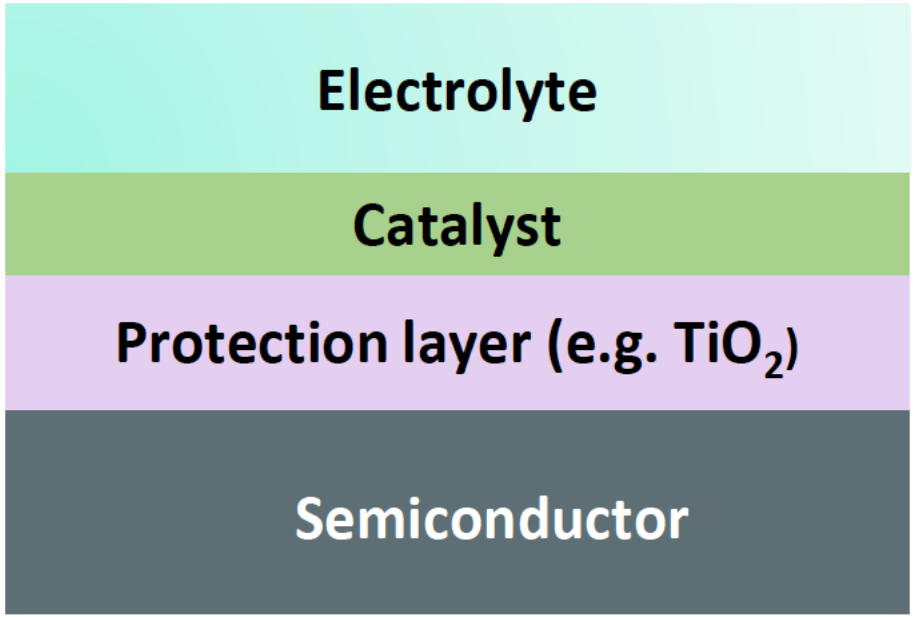

9.1. Panel-type CELLS

Record efficiency of solar-hydrogen production: 16.2 %

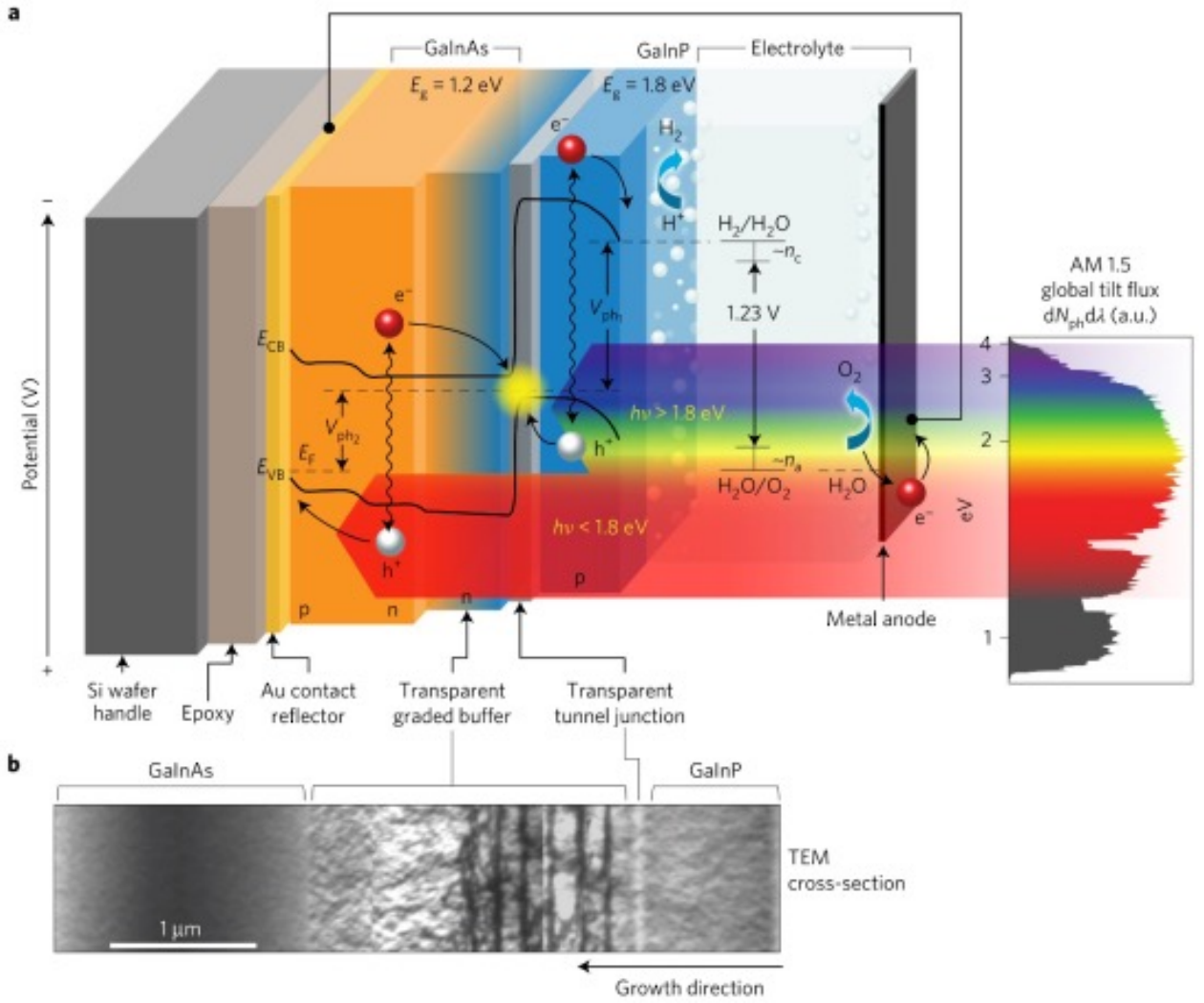

Turner, Deutsch, Nature Energy (2017)

9.1. Panel-type CELLS

ADVANCED ENERGY MATERIALS

Communication

Over 17% Efficiency Stand-Alone Solar Water Splitting Enabled by Perovskite-Silicon Tandem Absorbers

Siva Krishna Karuturi, Heping Shen, Astha Sharma, Fiona J. Beck, Purushothaman Varadhan, The Duong, Parvathala Reddy Narangari, Doudou Zhang, Yimao Wan, Jr-Hau He ... See all authors

Realizing solar-to-hydrogen (STH) efficiencies close to 20% using low-cost semiconductors remains a major step toward accomplishing the practical viability of photoelectrochemical (PEC) hydrogen generation technologies. Dual-absorber tandem cells combining inexpensive semiconductors are a promising strategy to achieve high STH efficiencies at a reasonable cost. Here, a perovskite photovoltaic biased silicon (Si) photoelectrode is demonstrated for highly efficient stand-alone solar water splitting. A p^+nn^+-Si/Ti/Pt photocathode is shown to present a remarkable photon-to-current efficiency of 14.1% under biased condition and stability over three days under continuous illumination. Upon pairing with a semitransparent mixed perovskite solar cell of an appropriate bandgap with state-of-the-art performance, an unprecedented 17.6% STH efficiency is achieved for self-driven solar water splitting. Modeling and analysis of the dual-absorber PEC system reveal that further work into replacing the noble-metal catalyst materials with earth-abundant elements and improvement of perovskite fill factor will pave the way for the realization of a low-cost high-efficiency PEC system.

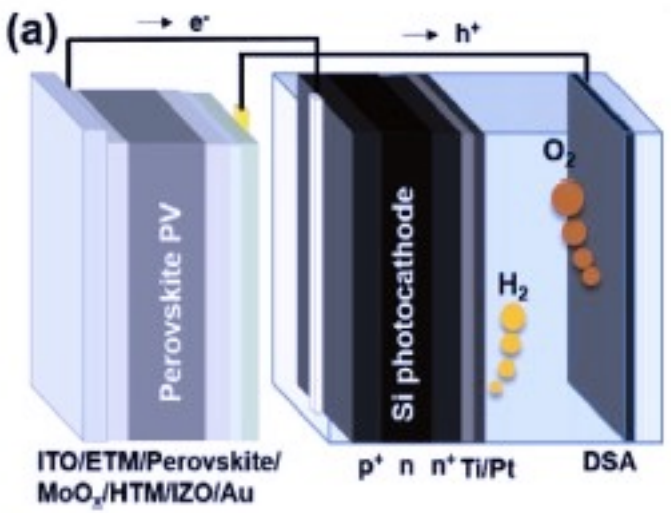

9.1. Panel-type CELLS

Which light absorbers are used?

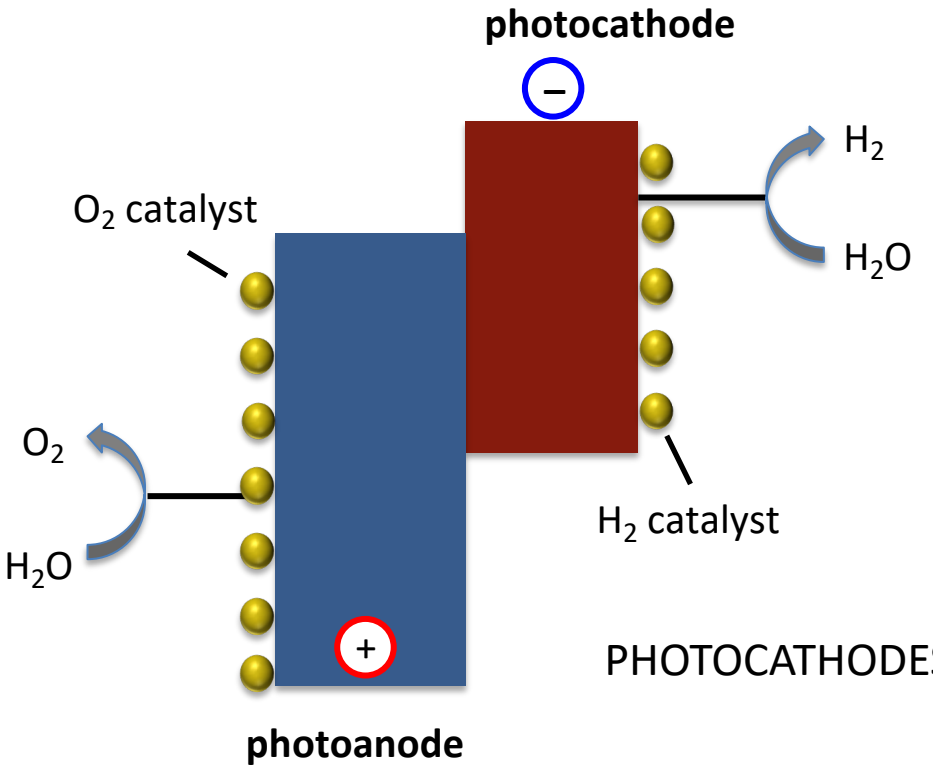

PHOTOCATHODES: Si, InP

PHOTOANODES: WO_3, α-Fe_2O_3, **$BiVO_4$**

Here it is the big problem and where nanostructuring can help!

9.1. Panel-type CELLS

Challenges with metal oxides

1. Absorption of earth-abundant MO photoanodes is limited to the uv and blue-tail of the spectrum

   (3.2 eV for anatase TiO_2 ; 3.3 eV for ZnO; 2.6eV- for WO_3)

2. Short hole diffusion length

   (from few nanometers to tens of nanometers for α-Fe_2O_3)

3. Indirect band gap

   (anatase TiO_2 ,WO_3, α-Fe_2O_3)

9.1. Panel-type CELLS

Why nanostructuring can be helpful?

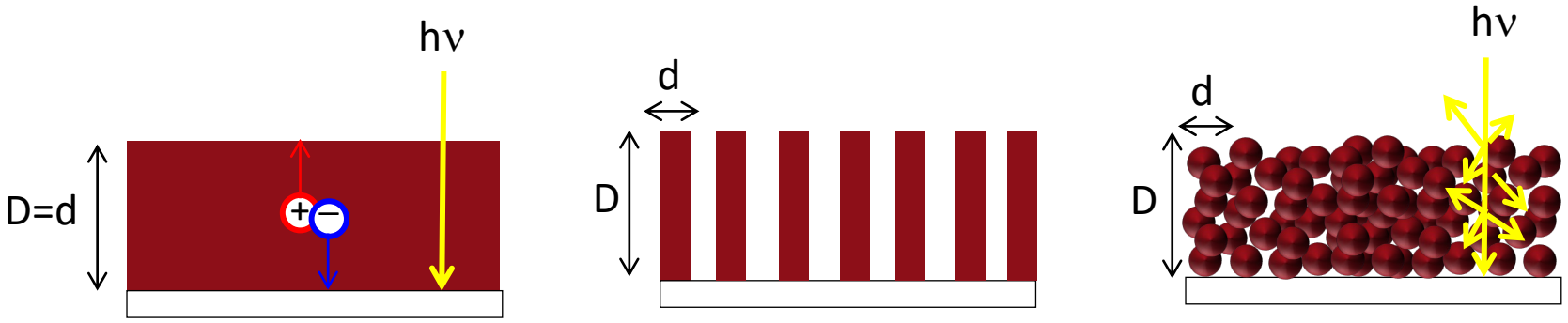

- Shorter carrier transport pathways
- Surface area-enhanced charge transfer
- Light trapping through random scattering

9.1. Panel-type CELLS

Nanostructuring in hematite

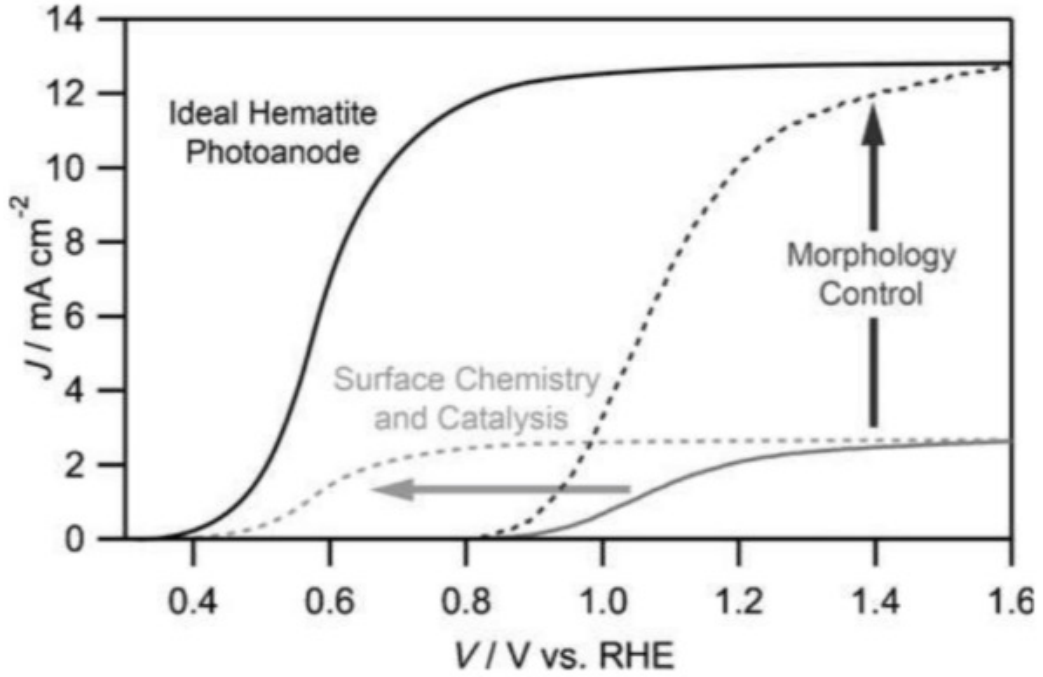

Figure 3. The two-part strategy for improving hematite performance is shown with respect to the photocurrent density, *J*, vs. voltage behavior for an idealized hematite photoanode (solid black trace) compared to the typical performance (solid grey trace) under AM 1.5G 100 mW cm^{-2} simulated sunlight, and the expected effects of improving the surface chemistry and the morphology.

Sivula et al. *Chem. Sus. Chem.* (**2011**)

9.1. Panel-type CELLS

Bismuth Vanadate

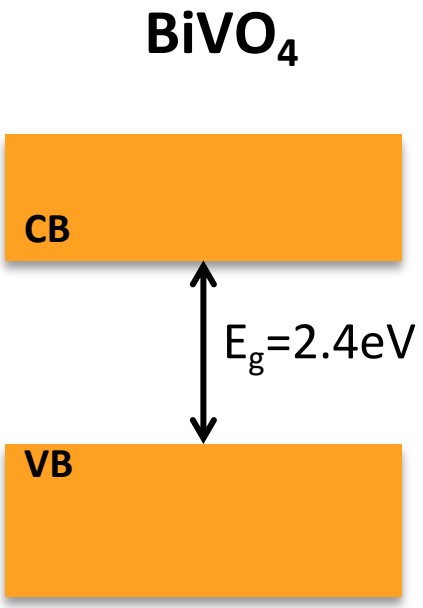

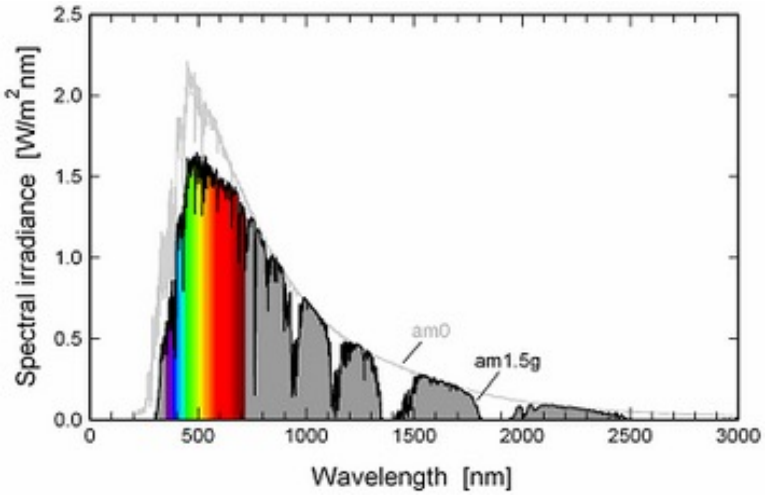

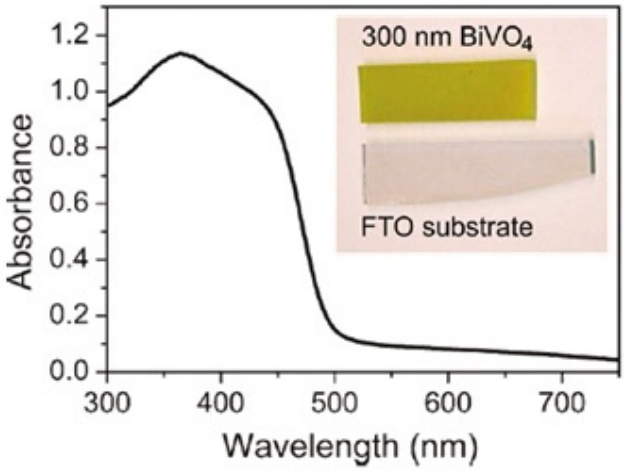

van de Krol et al. J. Phys. Chem. C (2011)

9.1. Panel-type CELLS

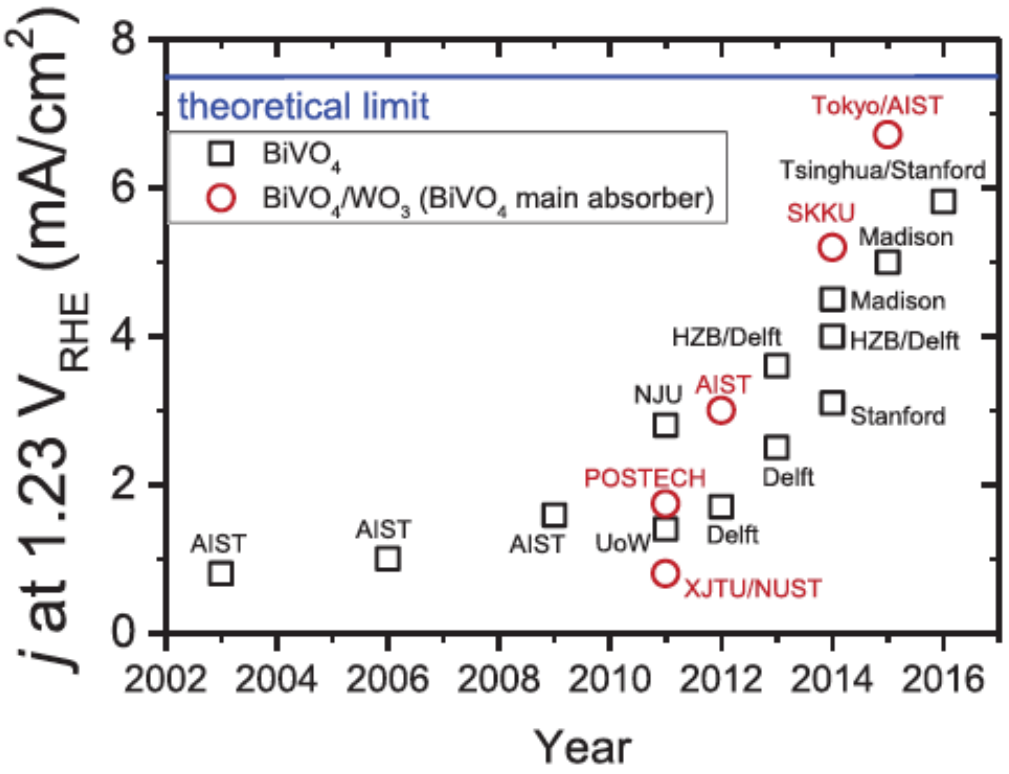

Figure 7. Reported photocurrent of $BiVO_4$ (black squares) and $BiVO_4/WO_3$ guest-host (red circles) photoanodes at 1.23 V versus RHE. Except for the first two points from AIST, the photocurrents were measured under AM1.5 illumination. Data were extracted from various reports in the literature [28, 31–33, 35–37, 56, 63–66, 73–79]. The theoretical maximum photocurrent for $BiVO_4$ based on its bandgap of 2.4 eV is shown as the horizontal blue line.

Abdi, Berglund, J. Appl. Phys. D (2017)

9.1. Panel-type CELLS

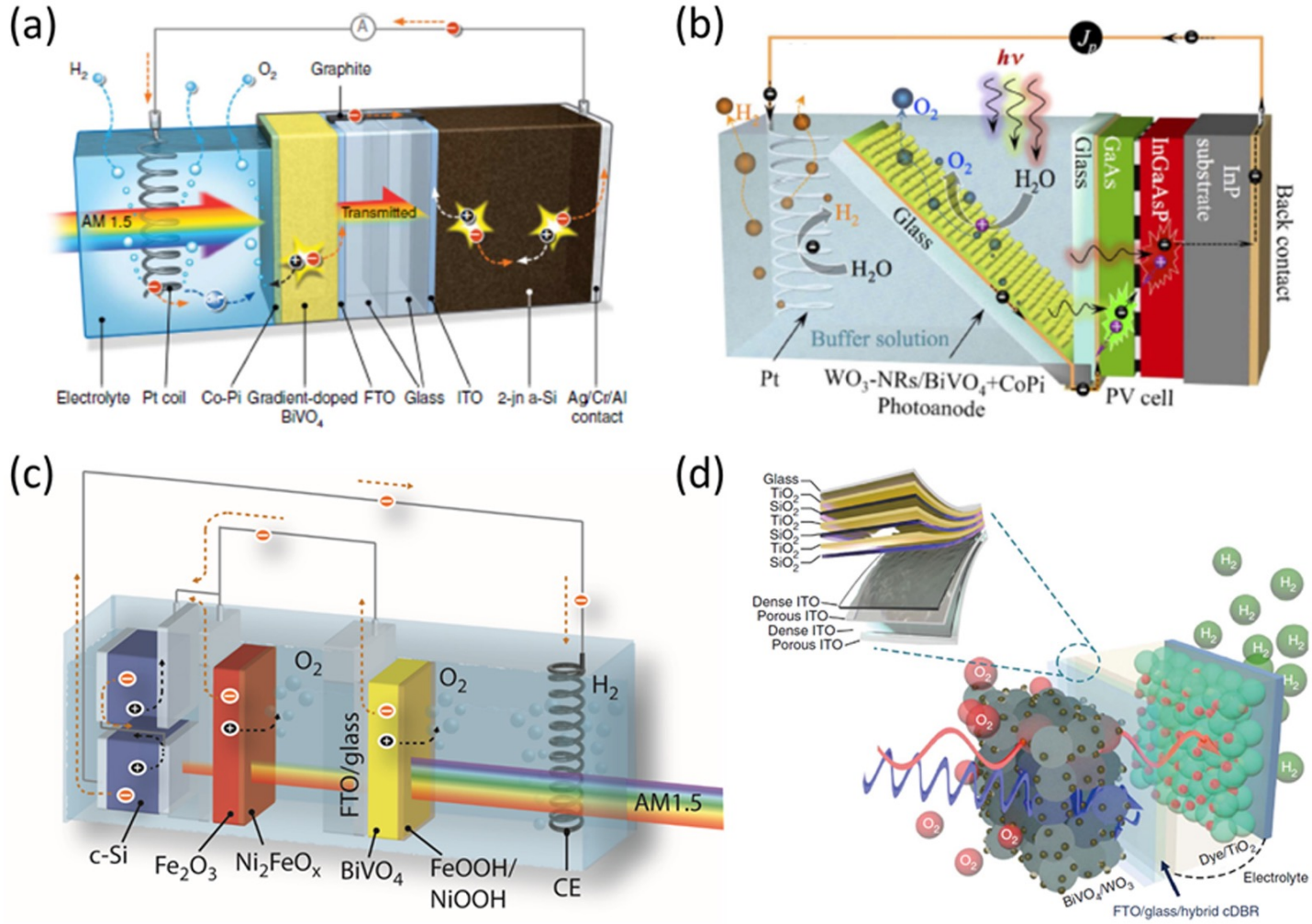

Various schematic structures of solar water splitting devices based on (a) BiVO4 photoanode and thin film amorphous silicon solar cell (b) BiVO4/WO3 nanorods photoanode and GaAs/InGaAsP solar cell, (c) BiVO4–Fe2O3 dual photoanode and crystalline silicon solar cell and (d) mesoporous BiVO4/WO3 photoanode, dye-sensitized solar cell (DSSC) and distributed Bragg reflector.

Abdi, Berglund, J. Appl. Phys. D (2017)

9.1. Panel-type CELLS

Record device with $BiVO_4$

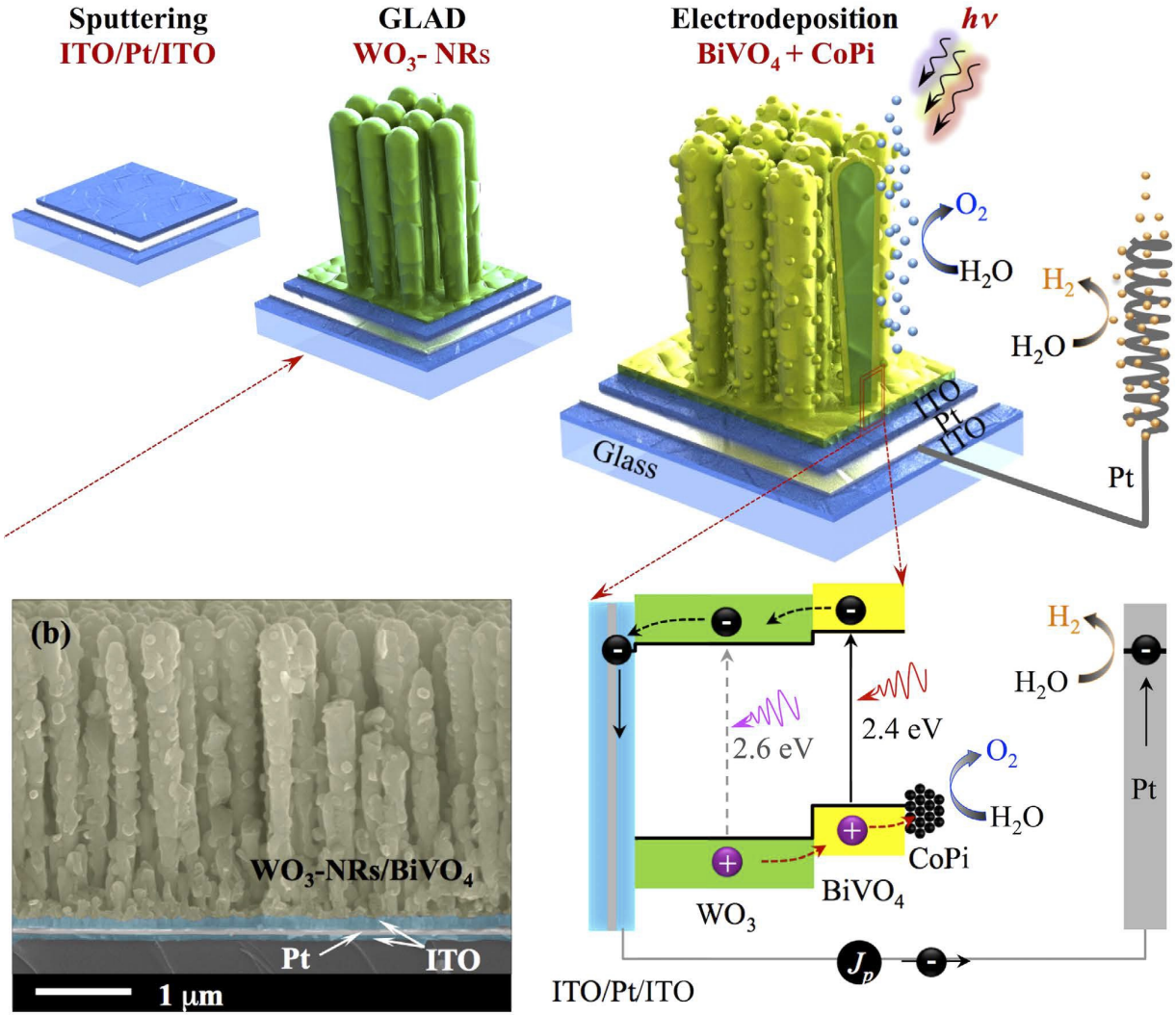

Kitamori et al. Sci. Rep. (2015)

9.1. Panel-type CELLS

BEYOND $BiVO_4$

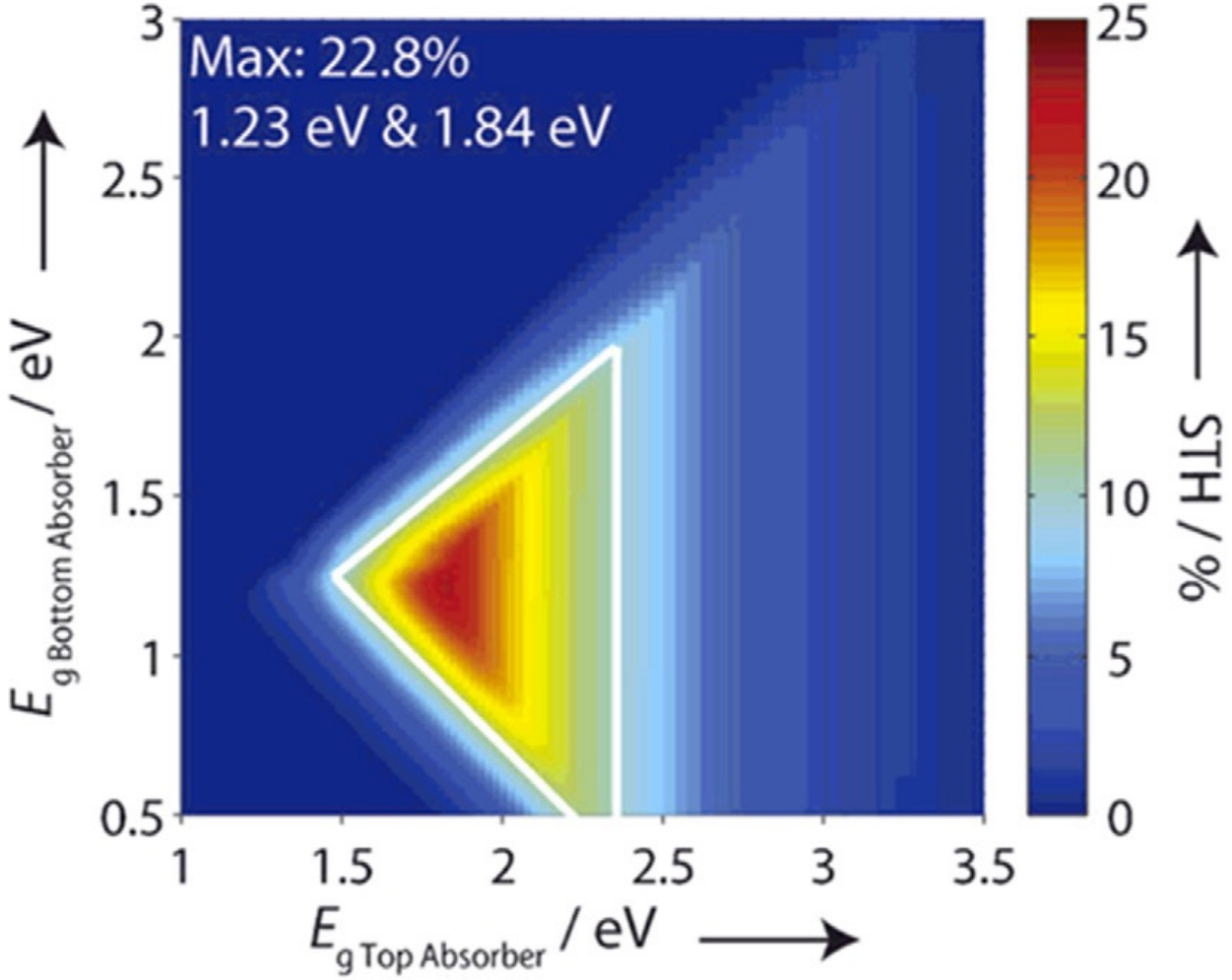

9.1. Panel-type CELLS

BEYOND $BiVO_4$: other metal vanadates with $E_g < 2\ eV$

FeV_2O_4 , Fe_2VO_4 , $Fe_2V_4O_{13}$

β-$Mn_2V_2O_7$

CuO– V_2O_5 system:

α-$Cu_2V_2O_7$, β-$Cu_2V_2O_7$,
γ-$Cu_3V_2O_8$, $Cu_{11}V_6O_{26}$

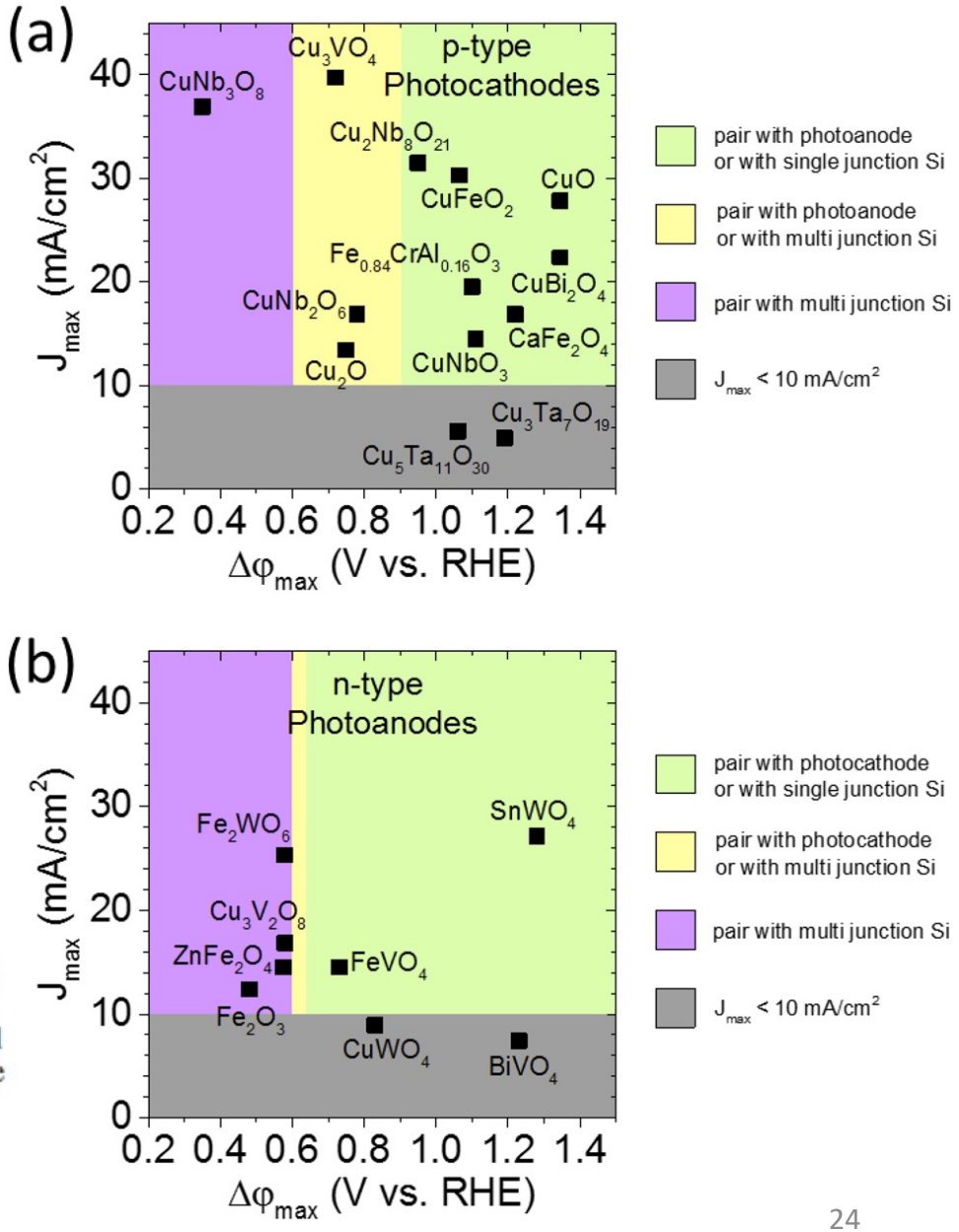

[redacted] Comparison of the J_{max} and $\Delta\varphi_{max}$ values for (a) p-type photocathode and (b) n-type photoanode materials. Regimes with different colors represent different categories. Grey indicates photocurrent maximum lower than 10 mA cm^{-2}. Green, yellow and magenta differentiate the most suitable tandem configuration for the material.

Abdi, Berglund, J. Appl. Phys. D (2017)

9.1. Panel-type CELLS

Nanocrystals to discover new materials

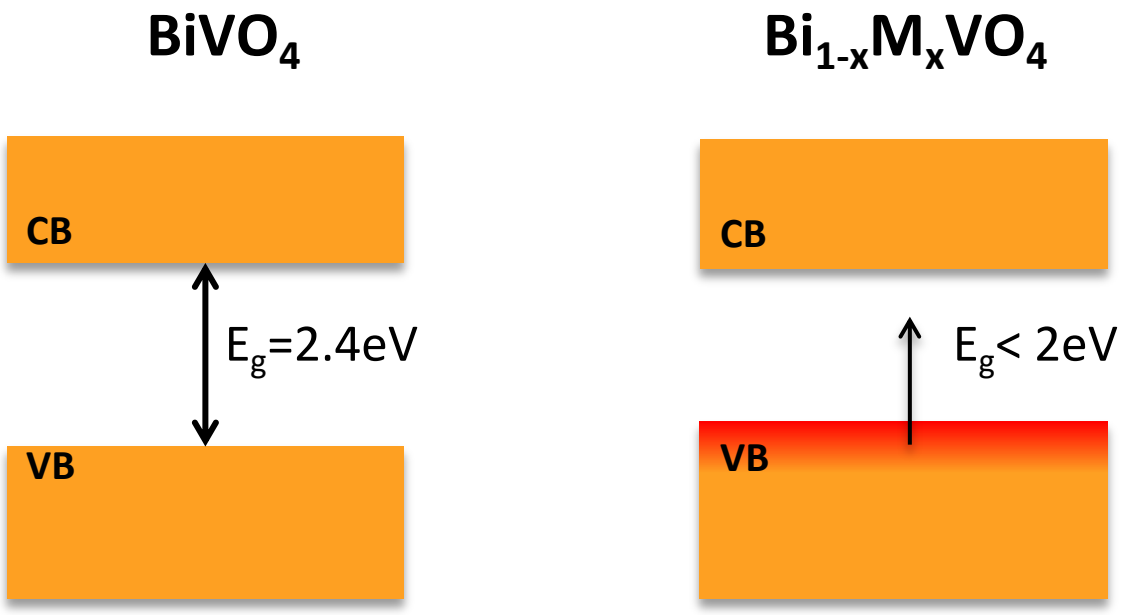

9.1. Panel-type CELLS

Nanocrystals to discover new materials

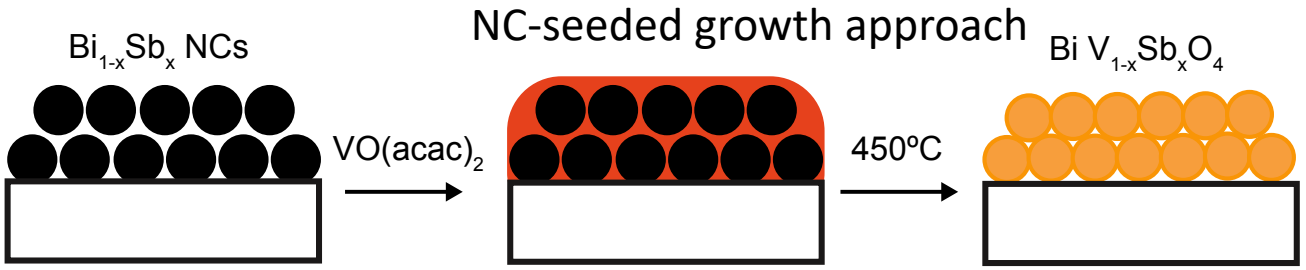

Representative TEM of $Bi_{1-x}Sb_x$ NCs

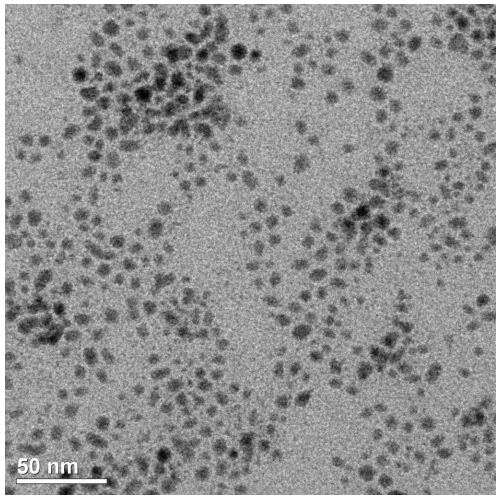

XRD of $Bi_{1-x}Sb_x$ NCs with variable composition

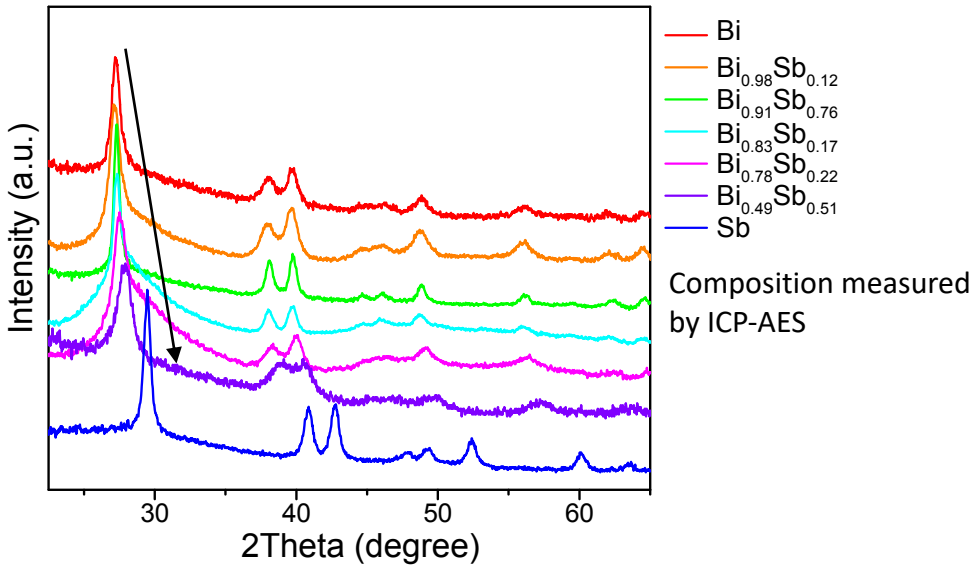

Loiudice et al. *Adv. Mater.* (**2015**) Zhang et al. *ACS Nano* (**2013**)

9.1. Panel-type CELLS

Nanocrystals to discover new materials

Sb-BVO films with up to 20% of Sb were obtained

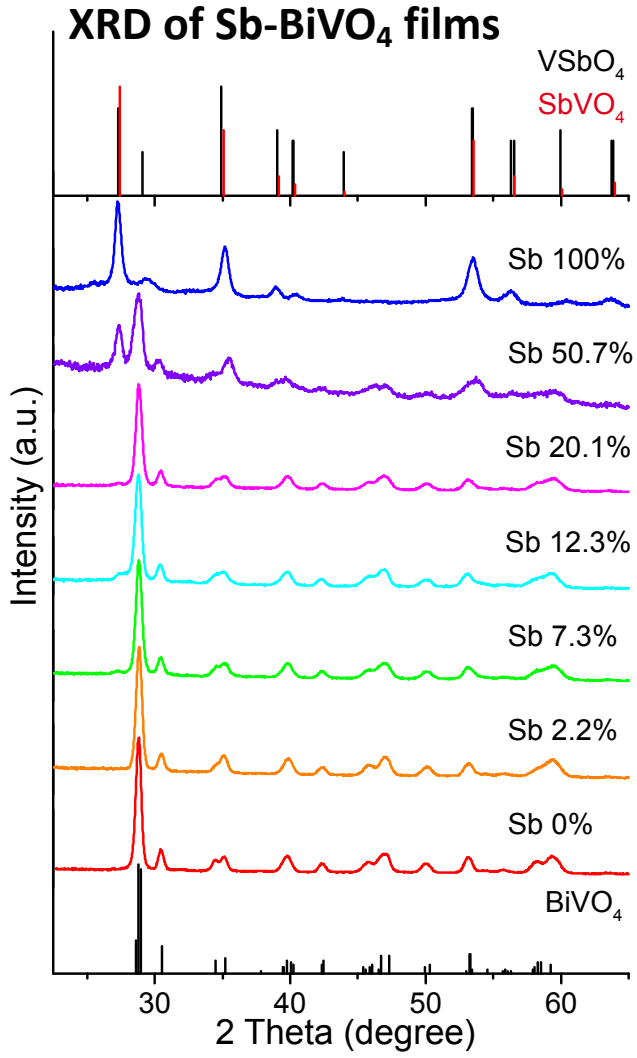

From Rietveld refinement

The monoclinic structure is preserved up to 20% Sb

70% $SbVO_4$ + 30% Sb_2VO_5

55% $SbVO_4$ + 45% $BiVO_4$

100% monoclinic $BiVO_4$

100% monoclinic $BiVO_4$

100% monoclinic $BiVO_4$

100% monoclinic $BiVO_4$

100% monoclinic $BiVO_4$

Loiudice et al. *Adv. Mater.* (**2015**)

The optical band gap decreases monotonically with the increase in Sb

Direct Band Gap

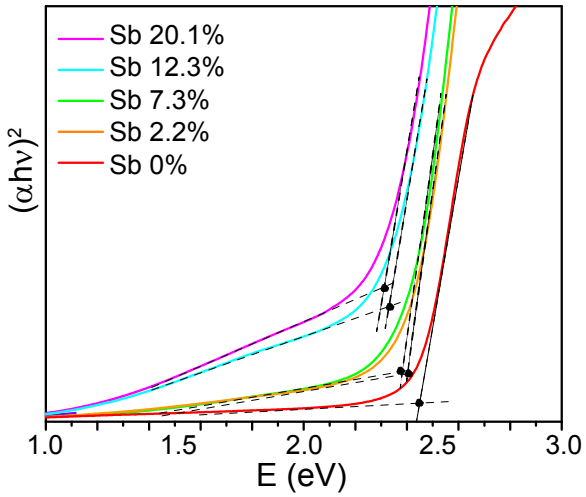

Indirect Band Gap

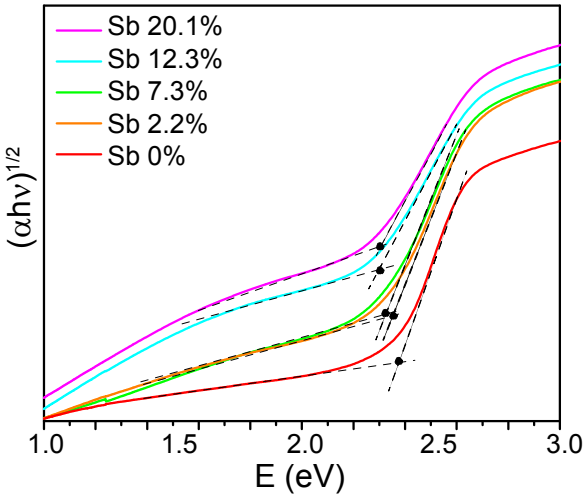

Eg	2.2 eV	←	2.45 eV	1.9 eV ← 2.3 eV
Sb	20.1%	←	0%	20.1% ← 0%

Loiudice et al. *Adv. Mater.* (**2015**)

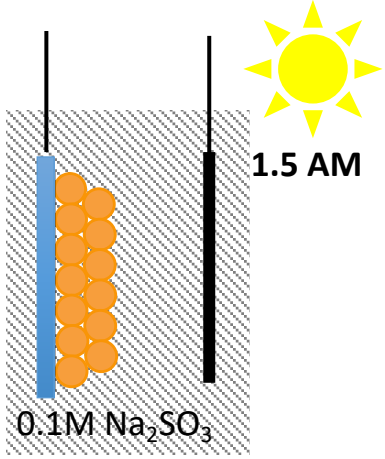

Photocatalytic performance improve with the increase of the Sb content

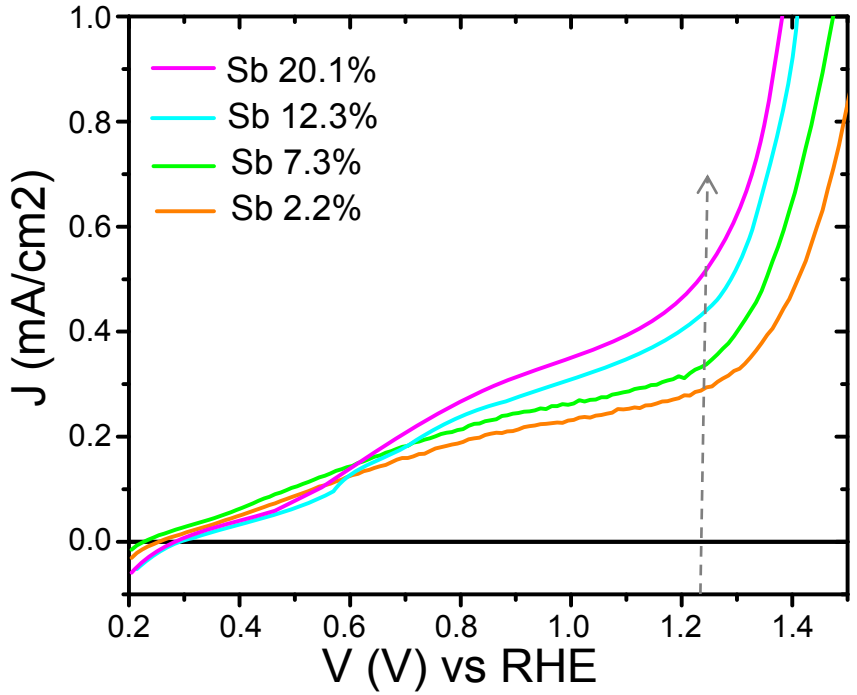

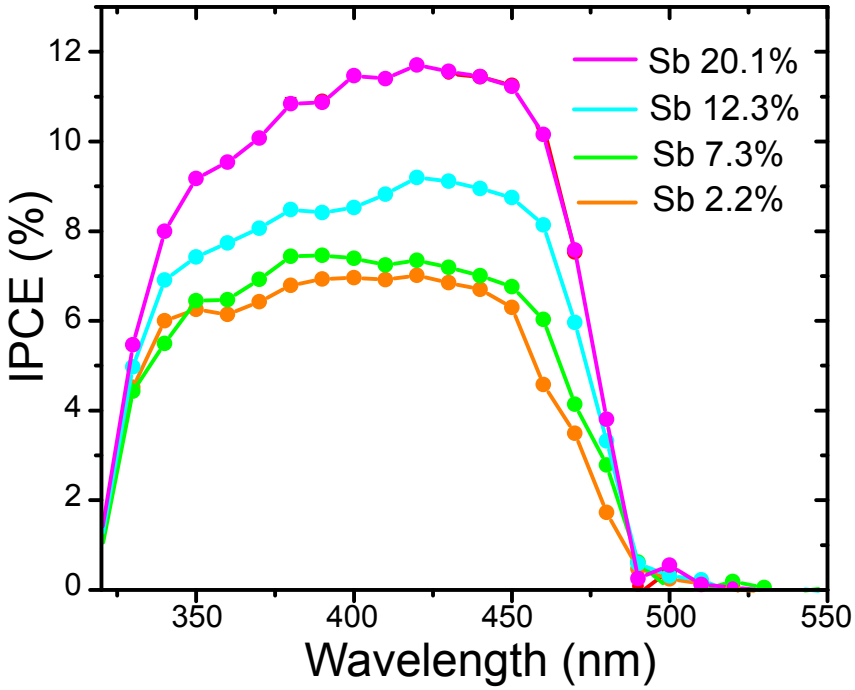

Loiudice et al. *Adv. Mater.* (**2015**)

BREAKTHROUGH 2023!!

Article

Solar-to-hydrogen efficiency of more than 9% in photocatalytic water splitting

https://doi.org/10.1038/s41586-022-05399-1

Received: 19 January 2021

Accepted: 29 September 2022

Published online: 4 January 2023

Check for updates

Peng Zhou[1], Ishtiaque Ahmed Navid[1], Yongjin Ma[1], Yixin Xiao[1], Ping Wang[1], Zhengwei Ye[1], Baowen Zhou[1], Kai Sun[2] & Zetian Mi[1]✉

Production of hydrogen fuel from sunlight and water, two of the most abundant natural resources on Earth, offers one of the most promising pathways for carbon neutrality[1–3]. Some solar hydrogen production approaches, for example, photoelectrochemical water splitting, often require corrosive electrolyte, limiting their performance stability and environmental sustainability[1,3]. Alternatively, clean hydrogen can be produced directly from sunlight and water by photocatalytic water splitting[2,4,5]. The solar-to-hydrogen (STH) efficiency of photocatalytic water splitting, however, has remained very low. Here we have developed a strategy to achieve a high STH efficiency of 9.2 per cent using pure water, concentrated solar light and an indium gallium nitride photocatalyst. The success of this strategy originates from the synergistic effects of promoting forward hydrogen–oxygen evolution and inhibiting the reverse hydrogen–oxygen recombination by operating at an optimal reaction temperature (about 70 degrees Celsius), which can be directly achieved by harvesting the previously wasted infrared light in sunlight. Moreover, this temperature-dependent strategy also leads to an STH efficiency of about 7 per cent from widely available tap water and sea water and an STH efficiency of 6.2 per cent in a large-scale photocatalytic water-splitting system with a natural solar light capacity of 257 watts. Our study offers a practical approach to produce hydrogen fuel efficiently from natural solar light and water, overcoming the efficiency bottleneck of solar hydrogen production.

A new leaf unfolds in artificial photosynthesis

Toyota Central R&D Labs is scaling up an efficient system that uses sunlight, water and carbon dioxide to produce important carbon compounds, paving a path to the practical use of artificial photosynthesis.

A cell with a solar-to-chemical conversion efficiency of 10.5% yields formate at a cost efficient production rate of 1.2 mole per hour.

In 2011, Toyota Central R&D Labs established a proof of principle for an artificial photosynthesis systems that produces carbon compounds from water, CO_2 and sunlight, without any other additives[3].

"Artificial photosynthesis, however, is very challenging," says Morikawa. Their first one square centimetre system used two photocatalysts immersed in water that, when exposed to sunlight, produced a ηSTC of 0.04%, only one fifth of the ηSTC demonstrated by a plant such as switchgrass. In 2015, however, continued improvements led to the 'artificial leaf', a one square centimetre electrode device that achieved a ηSTC of 4.6%, exceeding that of typical plants.

The team aspires to establish technology for an industrial system at a scale of one square metre by the 2030s. "The focus is to improve the system so that it captures and converts high-concentrate CO_2 from industrial emissions," says Kato.

9.0. Introduction and motivation

Panel-based or particle-based water splitting devices?

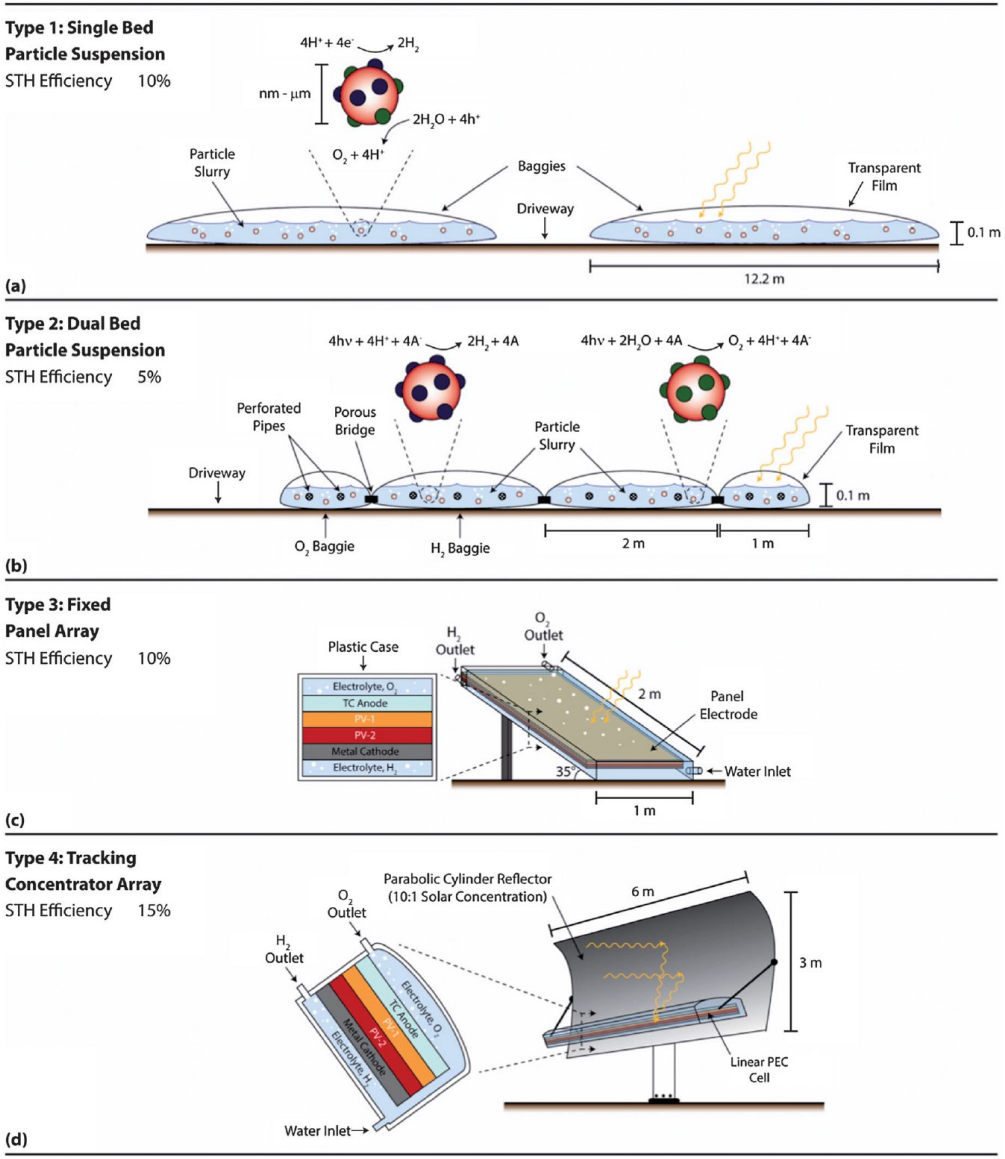

Jaramillo et al. Energy Environ Sci (2013)

9.2. Particle-based reactors

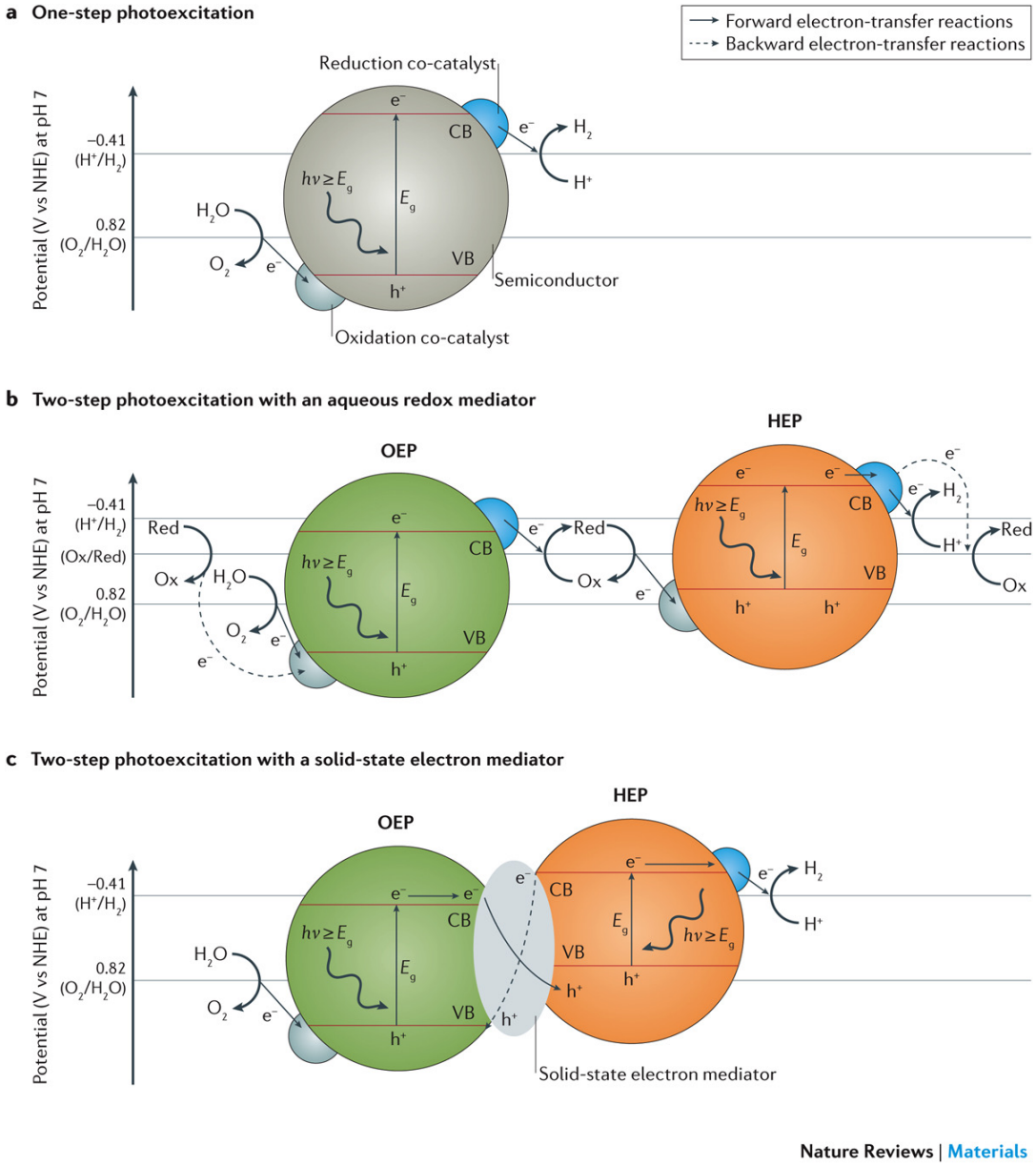

Domen et al. Nature Materials (2017)

9.2. Particle-based reactors

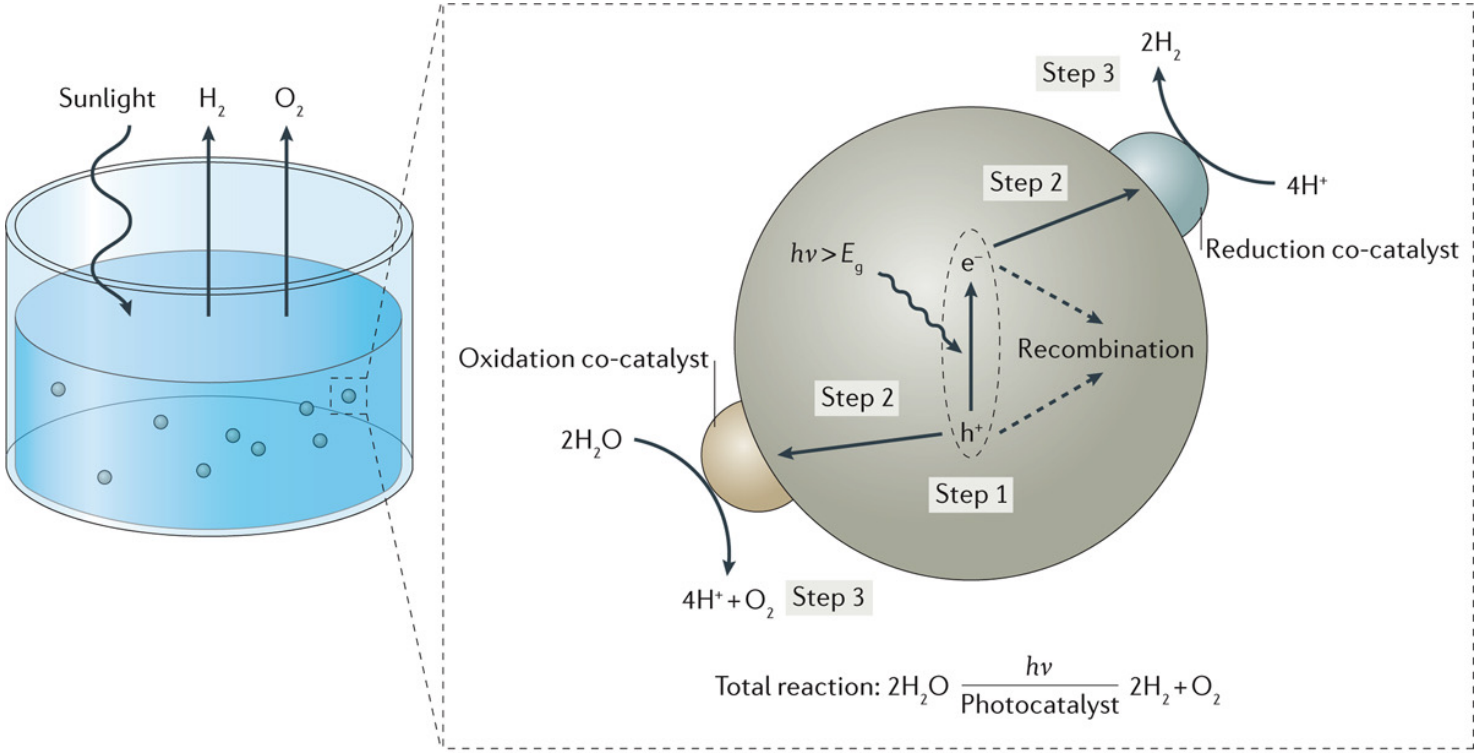

Domen et al. Nature Materials (2017)

9.2. Particle-based reactors

METRICS IN PARTICULATE PHOTOCATALYSIS:

External Quantum Efficiency (EQE) or Apparent Quantum Yield (AQE) is defined as two times the rate of collection of H_2 to the incident photon flux.

The solar-to-hydrogen (STH) energy conversion efficiency indicates the conversion of the energy in the incident solar irradiation to chemical bonds as H_2 through oxidation of water to O_2

9.2. Particle-based Reactors

Table 1 | Representative particulate one-step photoexcitation systems for overall water splitting

Semiconductor (available wavelength)	Co-catalyst	Surface modification	Light source	Reactant solution	Efficiency*	Refs
Ultraviolet light						
$SrTiO_3$:Al (<390 nm)	$Rh_{2-y}Cr_yO_3$ (Rh 0.1 wt%, Cr 0.1 wt%)	–	300 W Xe lamp (>300 nm)	H_2O	AQY: 30% at 360 nm	64
Ga_2O_3:Zn (<280 nm)	$Rh_{2-y}Cr_yO_3$ (Rh 1.0 wt%, Cr 1.5 wt%)	–	450 W Hg lamp	0.001 M $CaCl_2$ aqueous solution	AQY: 71% at 254 nm	65
$NaTaO_3$:La (<300 nm)	0.2 wt% NiO	–	400 W Hg lamp	H_2O	AQY: 56% at 270 nm	56
Ge_3N_4 (<340 nm)	1 wt% RuO_2	–	450 W Hg lamp	H_2O (pH = 0, H_2SO_4 mediated)	AQY: 9% at 300 nm	152
Visible light						
$(Zn_{1.12}Ge_{0.88})(N_{0.88}O_{0.12})$ (<475 nm)	$Rh_{2-y}Cr_yO_3$ (Rh 1.0 wt%, Cr 1.5 wt%)	–	450 W Hg lamp (>400 nm)	H_2O (pH = 4.5, H_2SO_4 mediated)	AQY: 5.9% at 420–440 nm	69, 153
GaN:Mg/InGaN:Mg (<475 nm)	Rh/Cr_2O_3	–	300 W Xe lamp (>400 nm)	H_2O	AQY: 12.3% at 400–475 nm, STH: 1.8%	6, 154
TaON (<495 nm)	3 wt% RuO_2/2.5 wt% Cr_2O_3–4 wt% IrO_2	ZrO_2	450 W Hg lamp (>400 nm)	H_2O	AQY: <0.1% at 420 nm	77
$LaMg_{1/3}Ta_{2/3}O_2N$ (<600 nm)	$Rh_{2-y}Cr_yO_3$ (Rh 0.5 wt%, Cr 0.5 wt%)	TiO_2/SiO_2	300 W Xe lamp (>420 nm)	H_2O	AQY: 0.18% at 440 ± 30 nm	68, 94
$SrTiO_3$:Rh,Sb (<500 nm)	3 wt% IrO_2	–	300 W Xe lamp (>440 nm)	H_2O (pH = 3, H_2SO_4 mediated)	AQY: 0.1% at 420 nm	75
CoO (<515 nm)	–	–	AM1.5G solar simulator	H_2O	STH: 5%	78
$BiYWO_6$ (<470 nm)	0.5 wt% RuO_2	–	500 W Xe lamp (>420 nm)	H_2O	AQY: 0.17% at 420 nm	80
$BiVO_4$:In,Mo (<496 nm)	3 wt% RuO_2	–	500 W Hg arc lamp (>420 nm)	H_2O	AQY: 3.2% at 420–800 nm	81
C_3N_4 (<442 nm)	3 wt% Pt–1 wt% CoO_x	–	300 W Xe lamp (>420 nm)	H_2O	AQY: 0.3% at 405 nm	84
CDots-C_3N_4 (<620 nm)	–	–	300 W Xe lamp (>420 nm)	H_2O	AQY: 16% at 420 nm, STH: 2%	52

AQY, apparent quantum yield; CDots, carbon nanodots; STH, solar to hydrogen. *AQY was measured at a specific wavelength or within a certain wavelength range.

Domen et al. Nature Materials (2017)

9.2. Particle-based Reactors

Table 2 | Representative particulate two-step overall water-splitting systems.

HEP (available wavelength)	OEP (available wavelength)	Electron mediator (V vs NHE)	Light source	Reactant solution	Efficiency	Refs
Aqueous redox mediator						
0.5 wt% Pt/TiO_2 (anatase, <387 nm)	TiO_2 (rutile, <410 nm)	IO_3^-/I^- (1.085 – 0.059 pH)	400 W high-pressure Hg lamp	H_2O (pH = 11, NaOH mediated)	No data	104
0.4 wt% Pt/$SrTiO_3$:(Cr,Ta) (<700 nm)	1 wt% PtO_x/WO_3 (<450 nm)	IO_3^-/I^- (1.085 – 0.059 pH)	300 W Xe lamp (>420 nm)	H_2O	AQY: 0.1% at 420 nm	110
1.0 wt% Pt/ZrO_2/TaON (<500 nm)	5 wt% Ir/TiO_2/Ta_3N_5 (<600 nm)	IO_3^-/I^- (1.085 – 0.059 pH)	300 W Xe lamp ($420 < \lambda < 800$ nm)	H_2O	No data	111
0.5 wt% Pt/ZrO_2/TaON (<500 nm)	0.5 wt% PtO_x/WO_3 (<450 nm)	IO_3^-/I^- (1.085 – 0.059 pH)	300 W Xe lamp ($420 < \lambda < 800$ nm)	H_2O	AQY: 6.3% at 420 nm	109
0.4 wt% Pt/$MgTa_2O_{6-x}N_y$/TaON (<570 nm)	0.45 wt% PtO_x/WO_3 (<450 nm)	IO_3^-/I^- (1.085 – 0.059 pH)	300 W Xe lamp ($420 < \lambda < 800$ nm)	H_2O	AQY: 6.8% at 420 nm	107
• 1 wt% Pt–2 wt% IrO_2/$Sm_2Ti_2S_2O_5$ (<590 nm): • 1 wt% Pt/$La_5Ti_2CuS_5O_7$ (<650 nm): • 1 wt% Rh/$La_6Ti_2S_8O_5$ (<630 nm)	0.45 wt% PtO_x/H-Cs-WO_3 (<450 nm)	I_3^-/I^- (0.536)	300 W Xe lamp (>420 nm)	H_2O	STH: 0.003%	98
Dye-adsorbed 0.5 wt% Pt/$H_4Nb_6O_{17}$ (<700 nm)	0.5 wt% IrO_2–0.5 wt% PtO_x/WO_3 (<450 nm)	I_3^-/I^- (0.536)	300 W Xe lamp (>420 nm)	H_2O (pH = 4.5, without adjustment)	AQY: 0.05% at 480 nm for H_2 evolution	101
3 wt% Pt/g-C_3N_4 (<442 nm)	0.5 wt% PtO_x/WO_3 (<450 nm) or $BiVO_4$ (<520 nm)	IO_3^-/I^- (1.085 – 0.059 pH) or Fe^{3+}/Fe^{2+} (0.771)	300 W Xe lamp (>395 nm)	H_2O (pH = 8.3) or H_2O (pH = 3.0, H_2SO_4 mediated)	No data	83
1 wt% Ru/$SrTiO_3$:Rh (<520 nm)	$BiVO_4$ (<520 nm)	Fe^{3+}/Fe^{2+} (0.771)	300 W Xe lamp (>420 nm)	H_2O (pH = 2.4, H_2SO_4 mediated)	AQY: 4.2% at 420 nm, STH: 0.1%	8
0.7 wt% Ru/$SrTiO_3$:Rh (<520 nm)	Bi_4NbO_8Cl (<498 nm)	Fe^{3+}/Fe^{2+} (0.771)	300 W Xe lamp (>420 nm)	H_2O (pH = 2.5, HCl mediated)	AQY: 0.4% at 420 nm for O_2 evolution	99

Domen et al. Nature Materials (2017)

9.2. Particle-based Reactors

ONE EXAMPLE

Scalable water splitting on particulate photocatalyst sheets with a solar-to-hydrogen energy conversion efficiency exceeding 1%

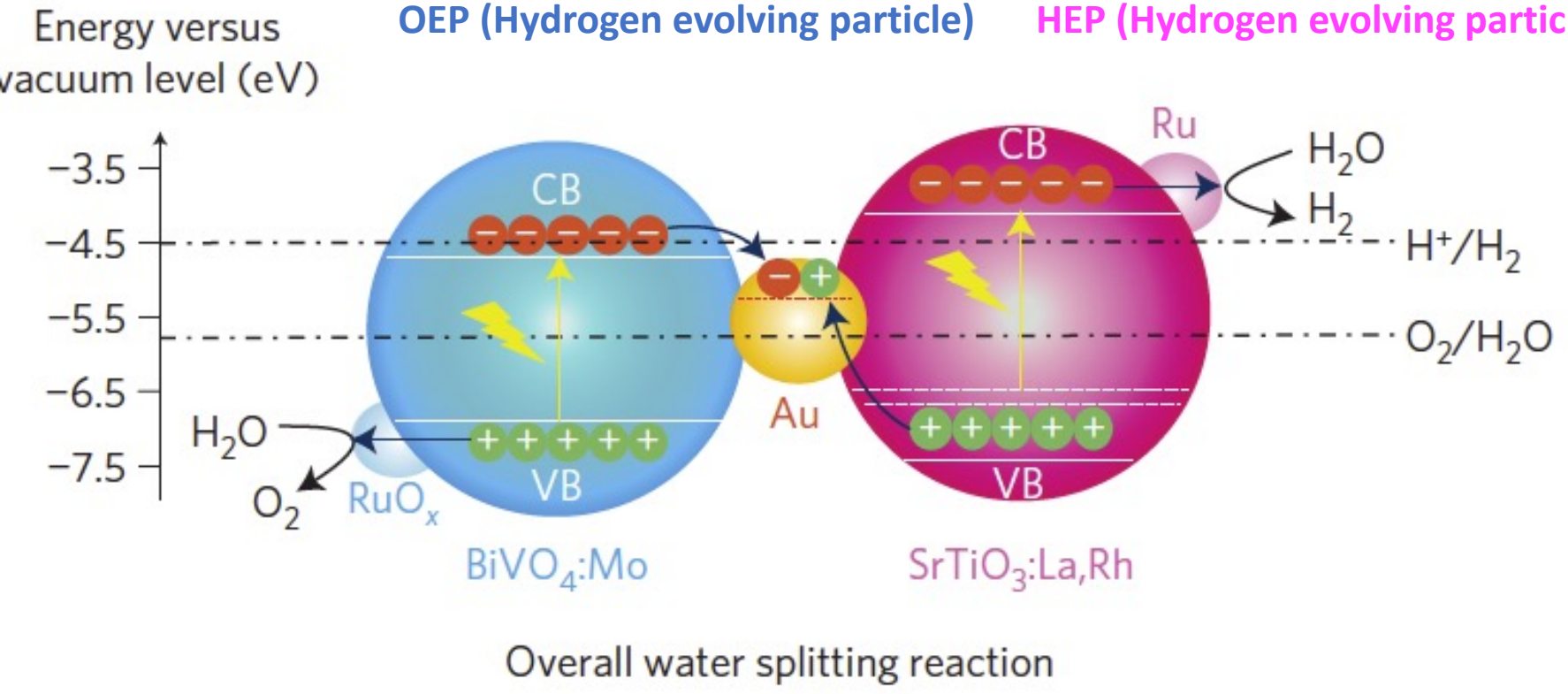

Domen et al. Nature Materials (2016)

9.2. Particle-based Reactors

ONE EXAMPLE

(I) Drop-casting of the mixture of OEP and HEP

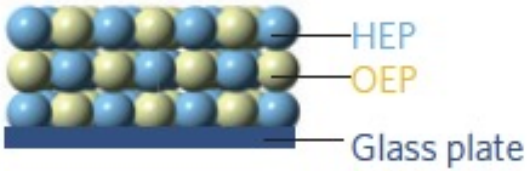

(II) Deposition of gold layer

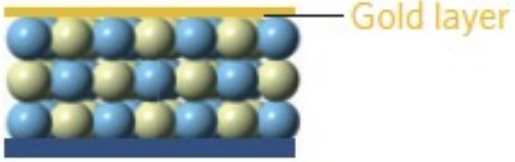

(III) Transfer of gold and particle layers

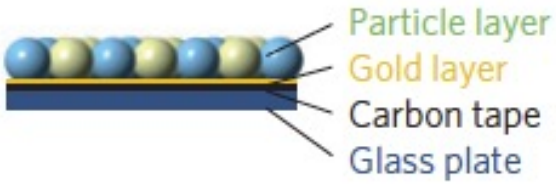

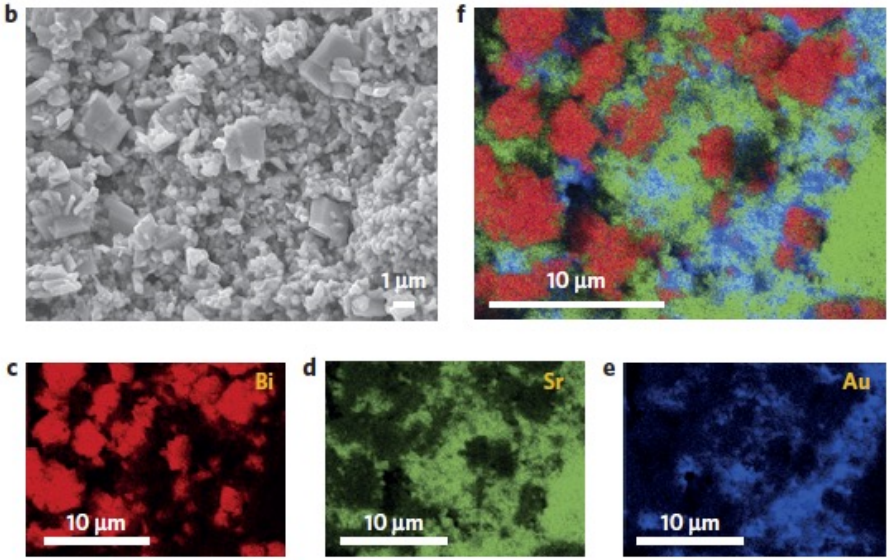

The HEP and OEP need to be in close proximity but not necessarily in contact. This is because, unlike in photoelectrochemical systems, a continuous conductive network is not needed, owing to the absence of an external electric circuit.

Domen et al. Nature Materials (2016)

9.2. Particle-based Reactors

ONE EXAMPLE

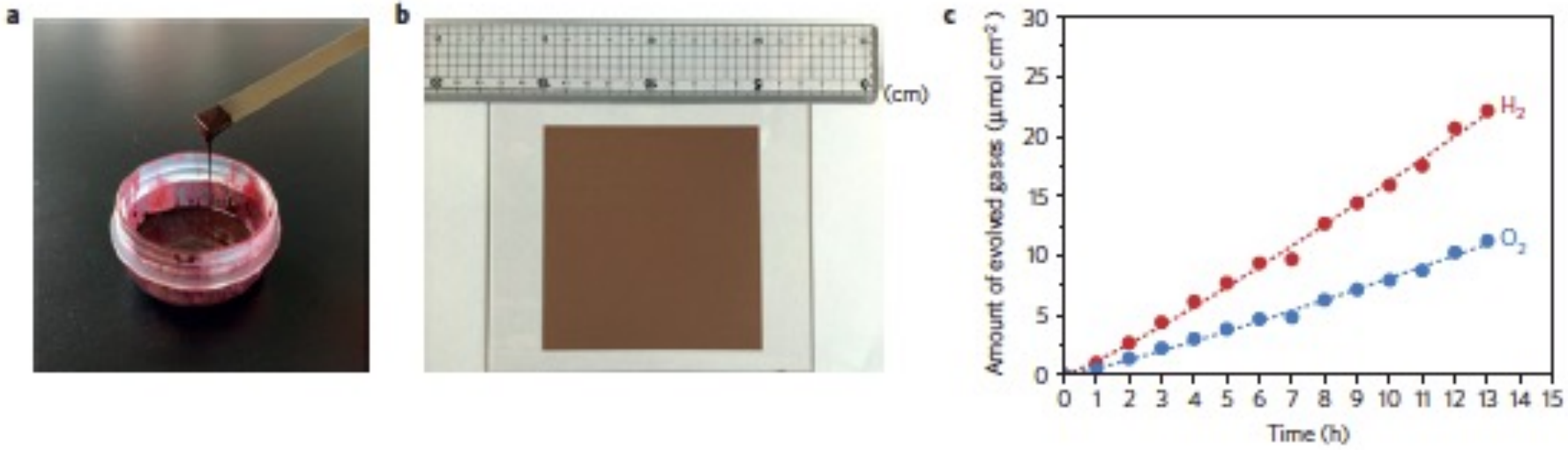

Figure 3 | Printed photocatalyst sheet. a, Photograph of the ink used for screen printing the photocatalyst sheet. **b**, Photograph of a 10 × 10 cm $SrTiO_3$:La,Rh/Au nanoparticle/$BiVO_4$:Mo printed sheet. **c**, Time course of the water splitting reaction using a Ru-modified $SrTiO_3$:La,Rh/Au colloid (40 wt%)/$BiVO_4$:Mo printed sheet under simulated sunlight at 288 K and 5 kPa. The sample (6.25 cm^2) was photodeposited with $RuCl_3 \cdot 3H_2O$ (0.17 μmol).

In conclusion, the authors demonstrate an efficient system based on nanoparticulate photocatalysts with AQE of 33%, STH of 1.1% in **pure water**

Domen et al. Nature Materials (2016)

Article

Photocatalytic solar hydrogen production from water on a 100-m² scale

https://doi.org/10.1038/s41586-021-03907-3

Received: 23 October 2020

Accepted: 12 August 2021

Hiroshi Nishiyama[1,10], Taro Yamada[1,10], Mamiko Nakabayashi[2], Yoshiki Maehara[3,4], Masaharu Yamaguchi[1], Yasuko Kuromiya[1], Yoshie Nagatsuma[1], Hiromasa Tokudome[3,5], Seiji Akiyama[3,6], Tomoaki Watanabe[7], Ryoichi Narushima[1], Sayuri Okunaka[3,5,9], Naoya Shibata[2], Tsuyoshi Takata[8], Takashi Hisatomi[8] & Kazunari Domen[1,8]✉

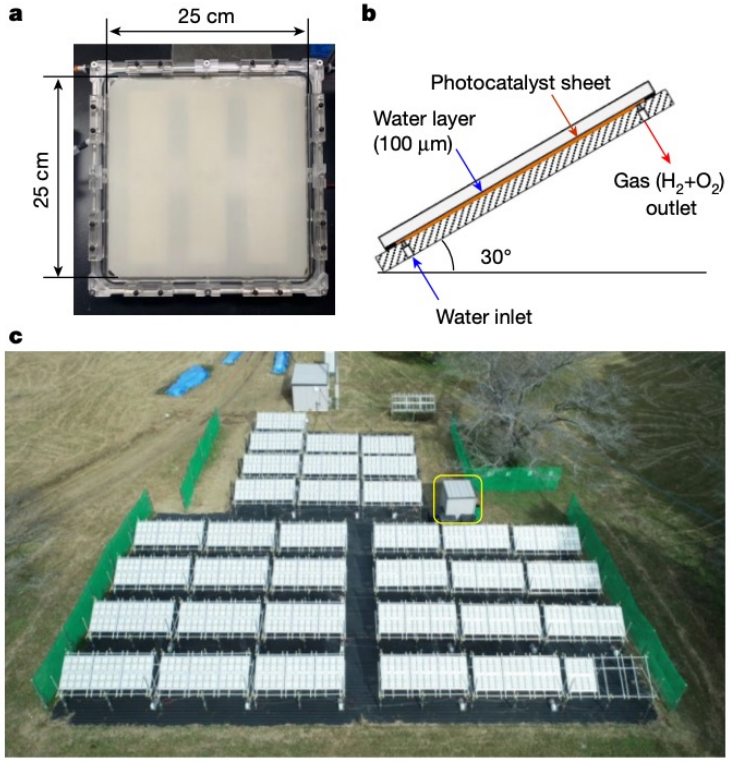

Fig. 1 | The 100-m² water splitting photocatalyst panel reactor. **a**, A photographic image of a panel reactor unit (625 cm²). **b**, The structure of the panel reactor unit viewed from the side. **c**, An overhead view of the 100-m² solar hydrogen production system consisting of 1,600 panel reactor units and a hut housing a gas separation facility (indicated by the yellow box).

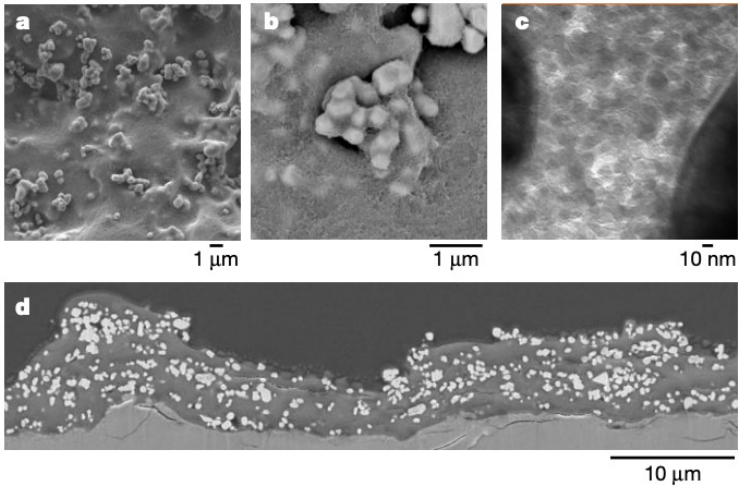

Fig. 2 | Electron microscopy images of photocatalyst sheets. **a**, **b**, Top-view secondary electron (**a**) and backscattered electron (**b**) images acquired by scanning electron microscopy. **c**, A cross-sectional image acquired by transmission electron microscopy. **d**, A cross-sectional backscattered electron image acquired by scanning electron microscopy. These specimens were fabricated by depositing the photocatalyst on frosted glass sheets using a program-controlled sprayer.

time and dropped below 0.40% in 280 h. Photocatalyst sheets fabricated on the frosted glass were more active and durable (Extended Data Fig. 4b), reaching after activation an STH efficiency of 0.51% that remained above 0.40% over 1,600 h (a timespan equivalent to seven months under an outdoor insolation of 7.6 kWh m^{-2} per day, or to almost

9.2. Particle-based Reactors

Hybrid colloidal nanocrystals for HER: model systems to understand structure/property relationships

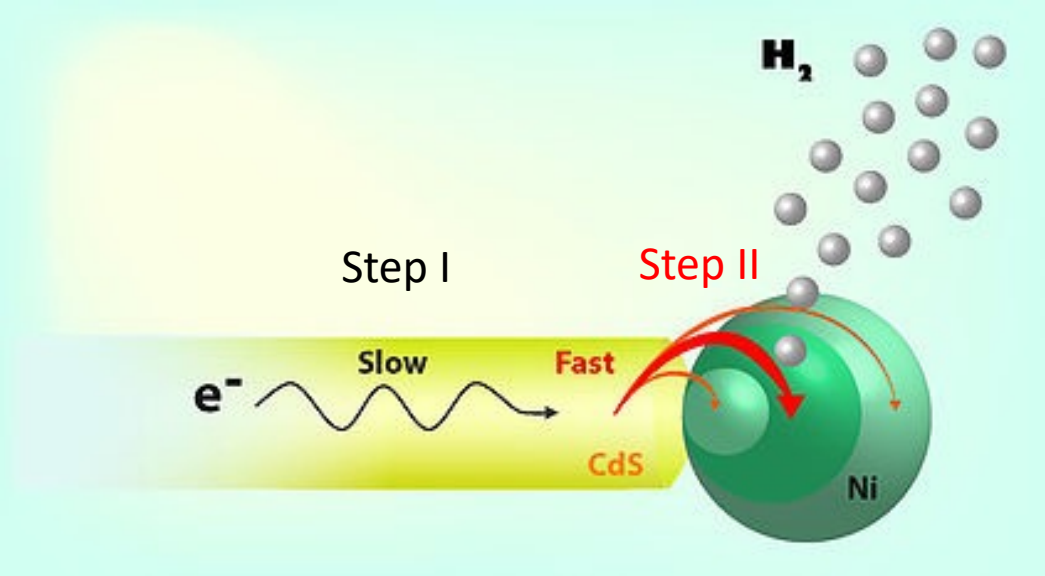

Step I (charge separation by diffusion)

Step II (interface crossing)

Is the size of the co-catalyst important to maximize HER?

Amirav et al. Nano Lett. (2018)

9.2. Particle-based photoelectrochemical reactors

Hybrid colloidal nanocrystals for HER

CdSe@CdS/Ni hybrids

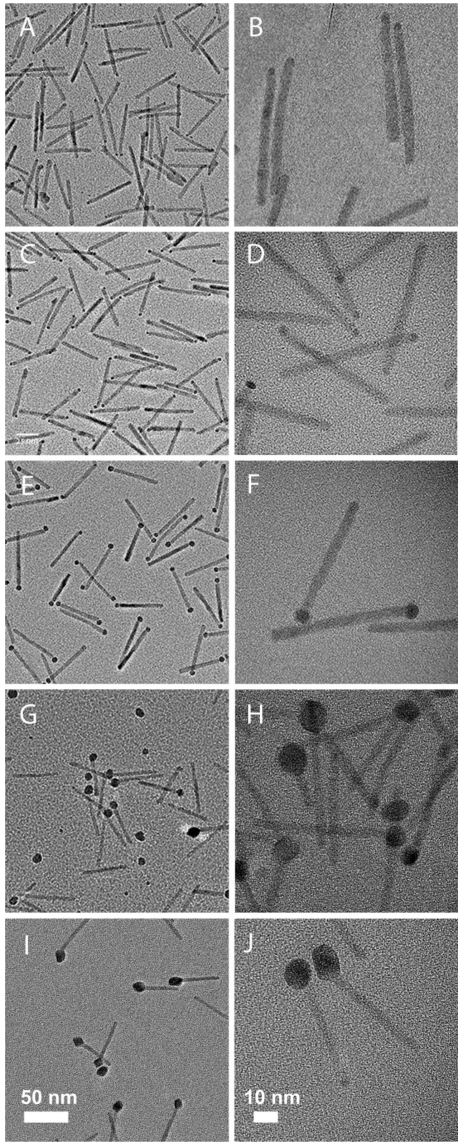

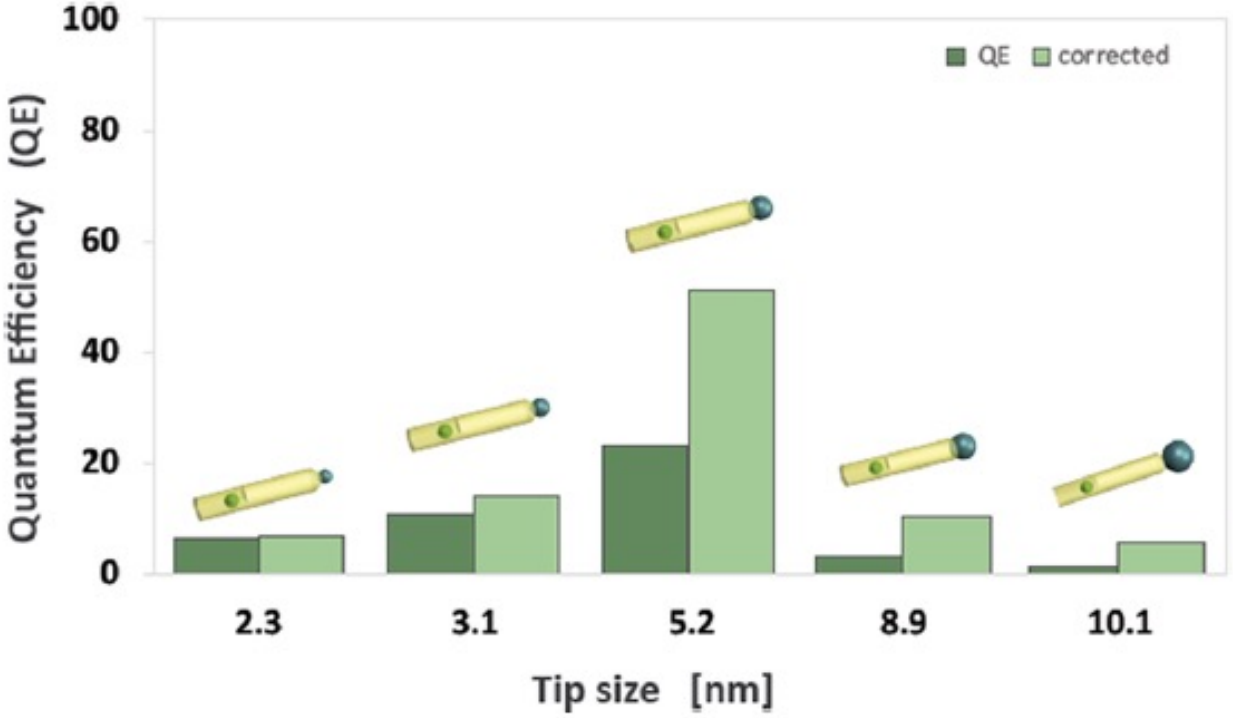

Figure 2. Photocatalytic quantum efficiency for the water reduction half reaction obtained with CdSe@CdS nanorod photocatalysts decorated with different-sized Ni tips. Experimental quantum efficiency in dark green bars, and quantum efficiency corrected for metal absorption in light green bars.

Amirav et al. Nano Lett. (2018)

9.2. Particle-based Reactors

Hybrid colloidal nanocrystals for HER: model systems to understand structure/property relationships

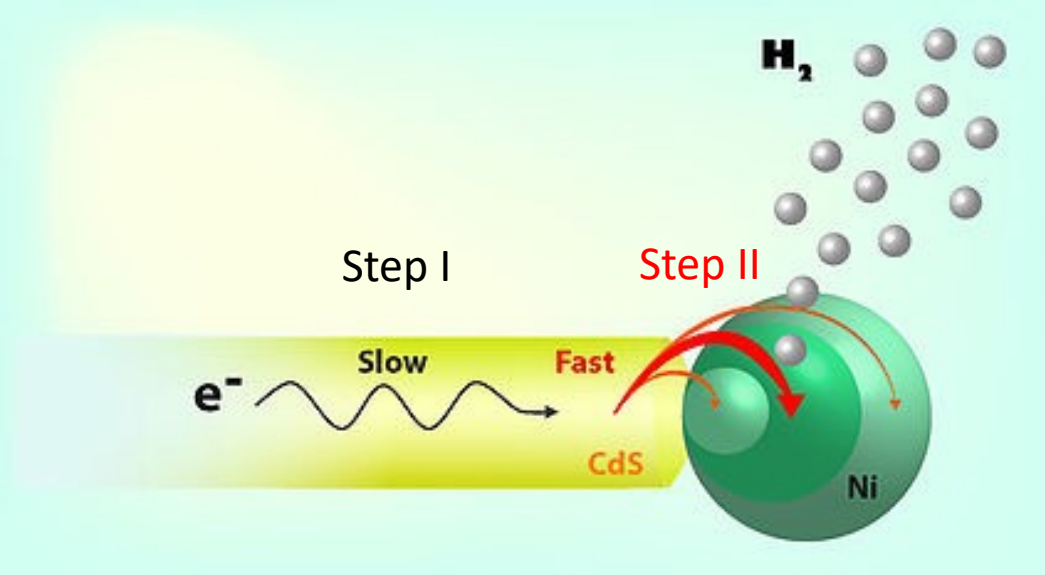

Step I (charge separation by diffusion) is not affected by the size of the co-catalyst

Step II (interface crossing) is affected by the size of the co-catalyst: the Coulomb blockade prevails at smaller sizes, the Schottky barrier at bigger sizes; the best is in the middle.

Amirav et al. Nano Lett. (2018)

9.2. Particle-based Reactors

Schottky junction

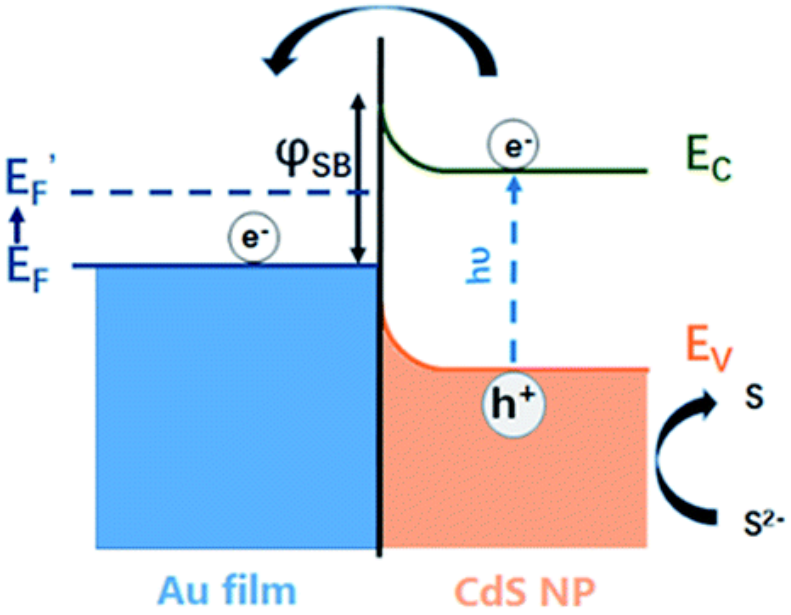

blue light excitation

Coulomb Blockade Effect:

The charging effect which blocks the injection of a single charge into or from a nanoparticles. This effect increases as the size becomes smaller

9.2. Particle-based Reactors

Hybrid colloidal nanocrystals for HER: model systems to understand structure/property relationships

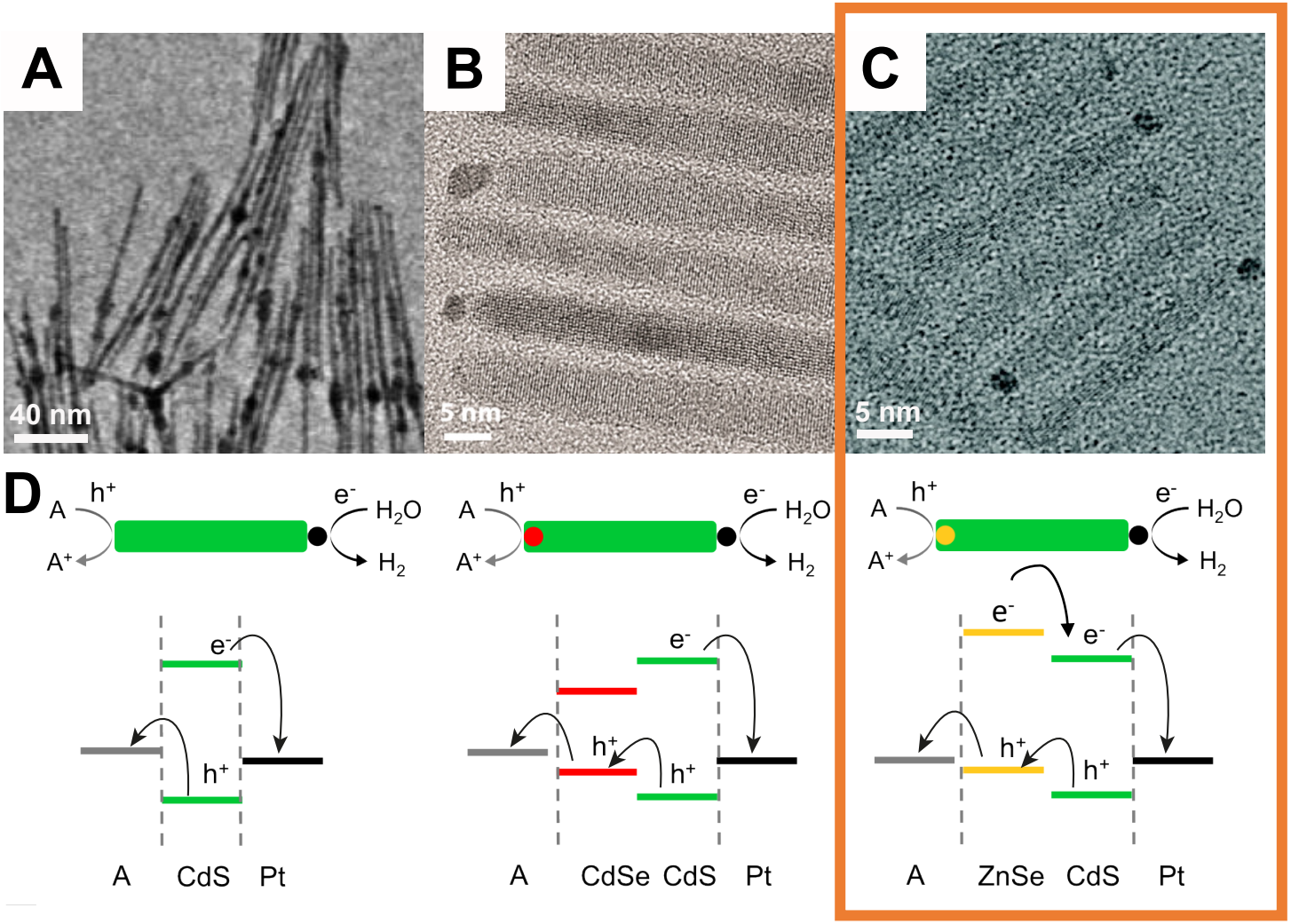

from Gadiyar et al. *J. Appl. Phys. D* (**2017**)

More light is absorbed and best band alignment

9.2. Particle-based Reactors

Coupling of semiconductor nanocrystals with enzymes

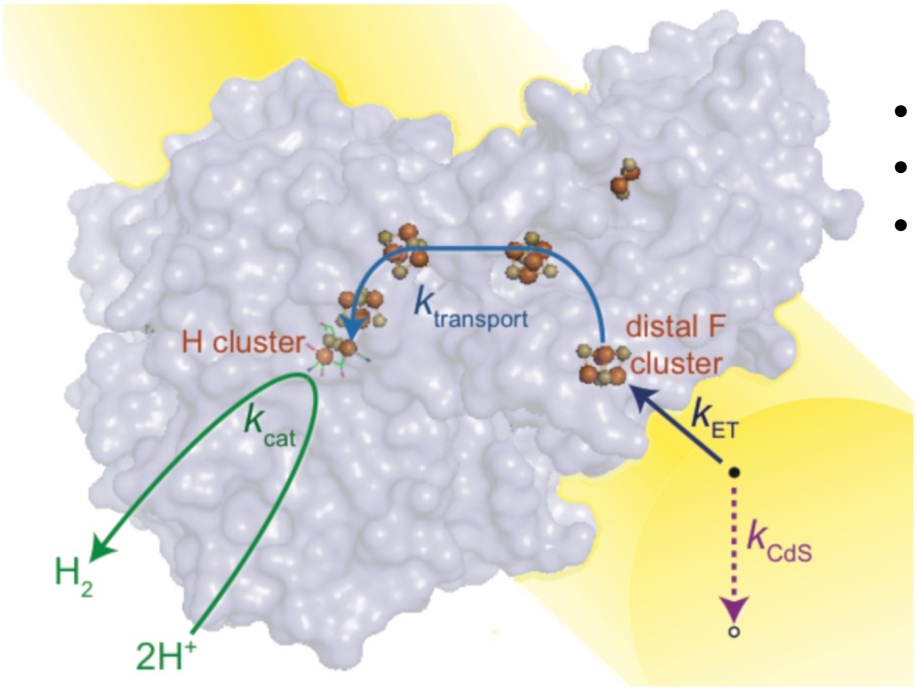

Figure 5. Schematic of the electron pathway resulting in H_2 generation by photoexcited CdS−CaI complexes. The enzyme surface is shown in blue with the Fe and S atoms of the F-clusters and the H-cluster shown as orange and yellow spheres, respectively. Enzyme coordinates are from CpI (PDB ID: 3C8Y), which has high homology and sequence similarity with CaI. The CdS NR surface is shown in yellow and surface-capping ligands are omitted for clarity. The rate of internal electron decay in CdS is denoted by k_{CdS}, the rate of electron injection from CdS to CaI by k_{ET}, the rate of electron transport through CaI to the H-cluster by $k_{transport}$, and the rate of H_2 production by k_{cat}.

- Photocatalyst: CdS
- Catalyst: Enzime
- Donor acceptor: Ascorbic acid

Dukovic et al. *JACS* (**2014**)

9.3. New concepts using nanomaterials

Plasmon-enabled photochemistry:
coupling of photonic and thermal stimuli to drive chemical transformation

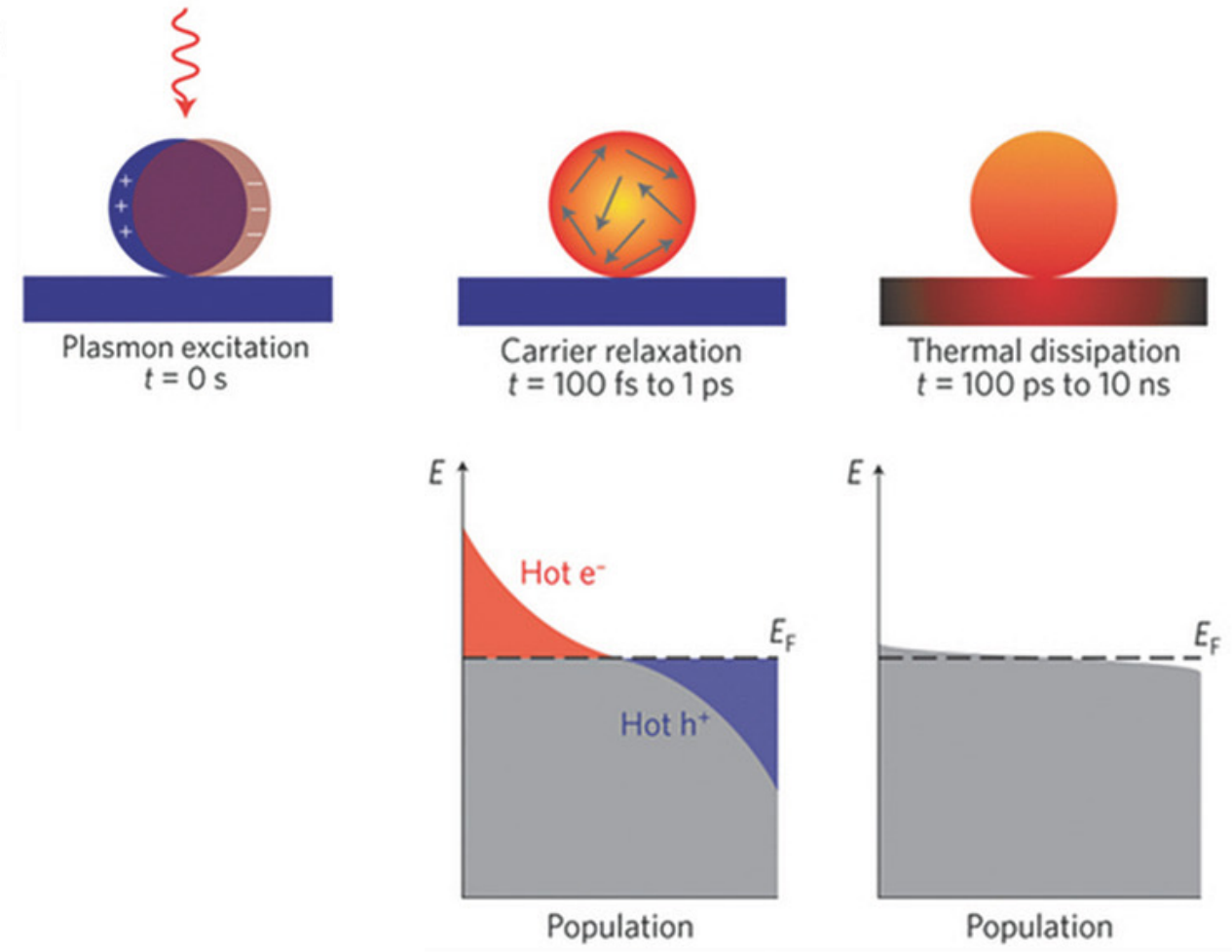

9.3. New concepts using nanomaterials

Plasmon-enabled photochemistry:
coupling of thermal and photonic stimuli to drive chemical transformation

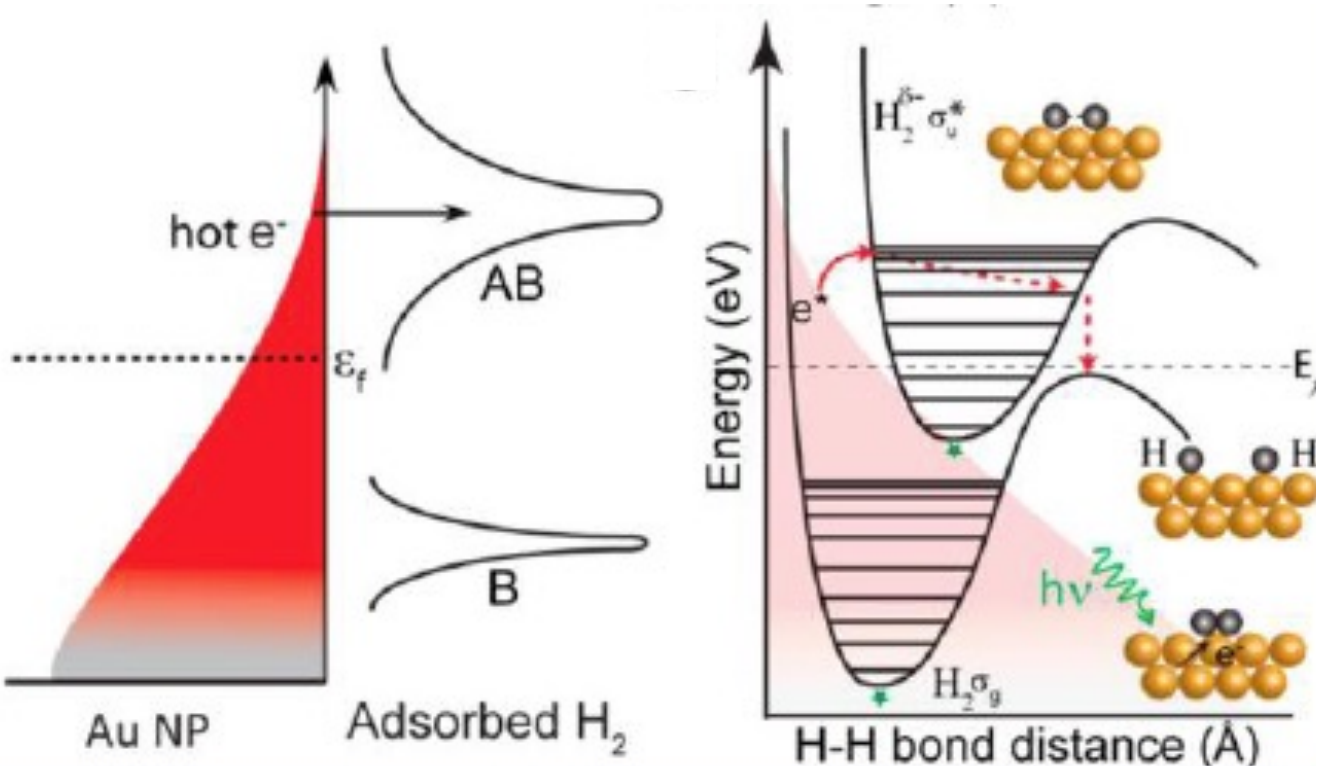

Halas Nano Lett. (2012); Linic Nature Chem (2011) and Nature Mater (2012)

9.3. New concepts using nanomaterials

Hot electron transfer to semiconductors to enhance activity

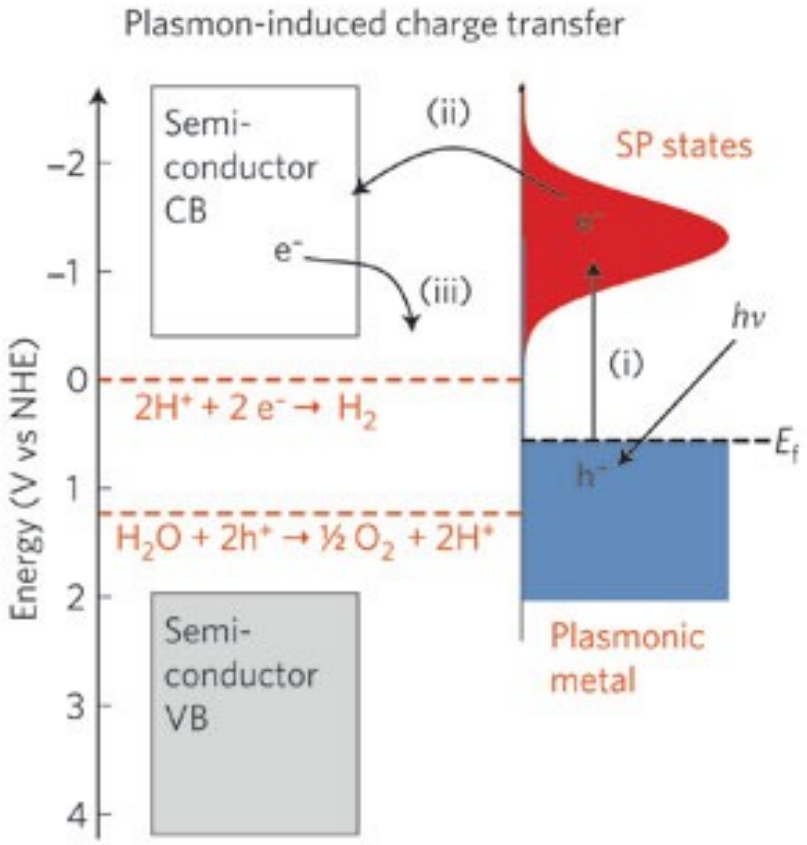

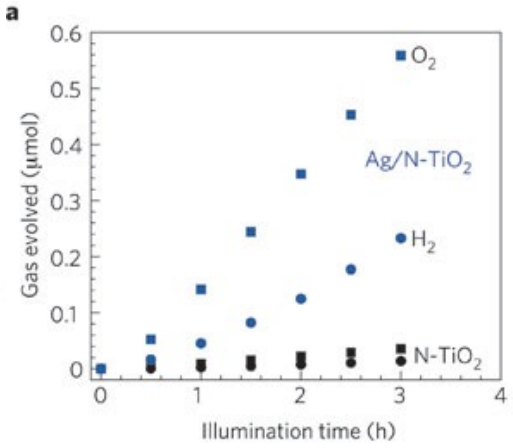

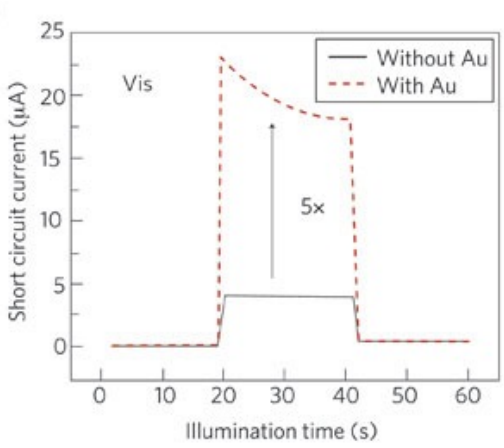

Nature Materials **2011**,10, 911

9.4. Beyond water splitting

Check for updates

Cite this: *Energy Environ. Sci.*, 2018, **11**, 2853

Received 14th May 2018,
Accepted 6th August 2018

DOI: 10.1039/c8ee01408f

rsc.li/ees

Plastic waste as a feedstock for solar-driven H_2 generation†‡

Taylor Uekert, [a] Moritz F. Kuehnel, *[ab] David W. Wakerley[a] and Erwin Reisner *[a]

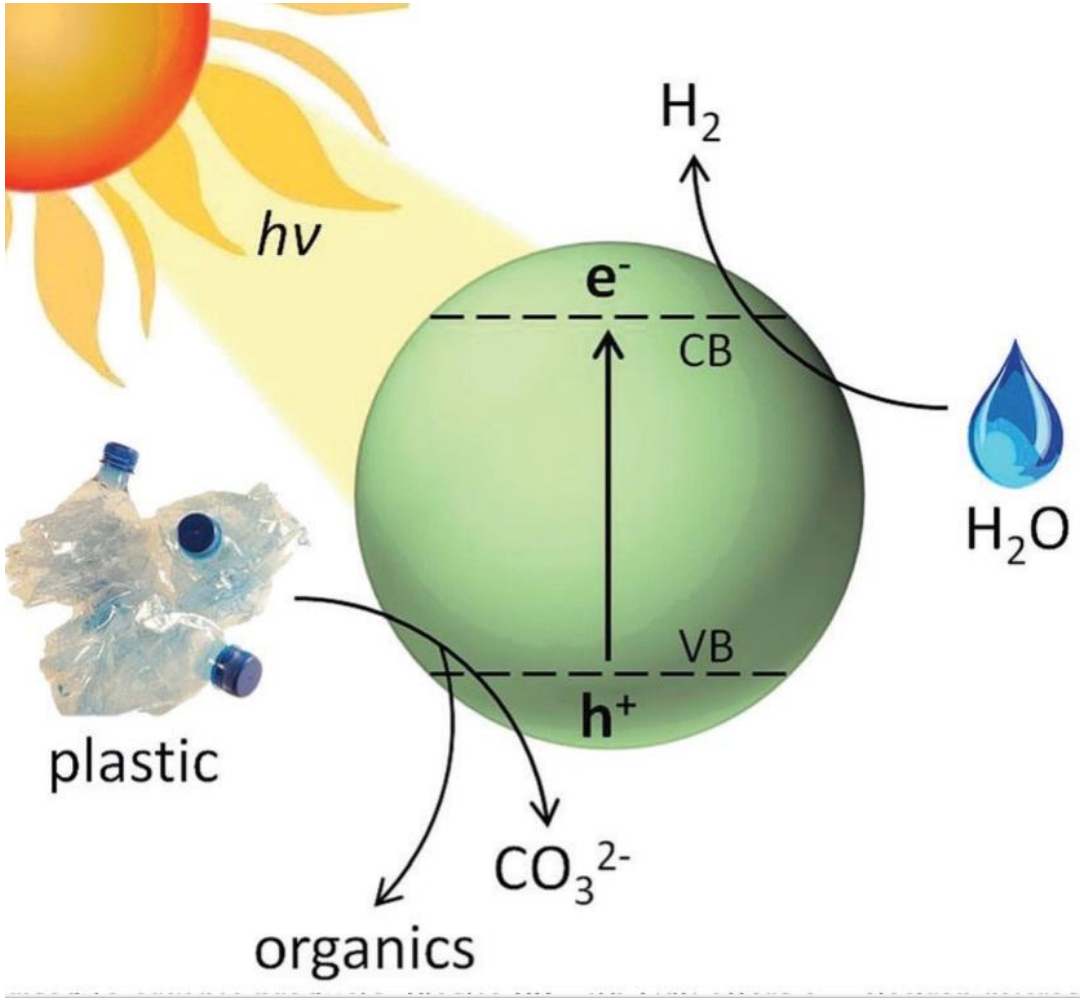

9.4. Beyond water splitting

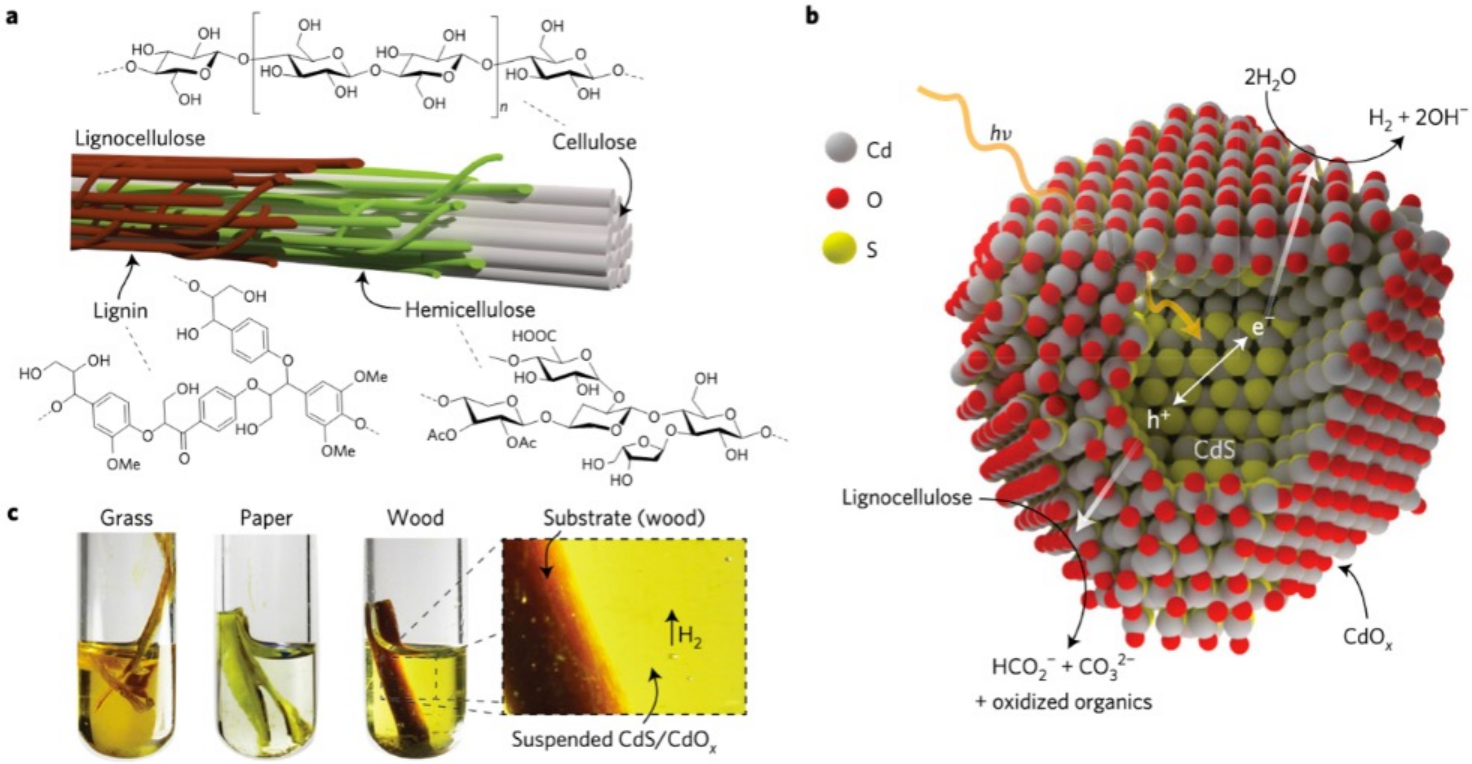

Solar-driven reforming of lignocellulose to H_2 with a CdS/CdO_x photocatalyst.

Wakerley, D. W.; Kuehnel, M. F.; Orchard, K. L.; Ly, K. H.; Rosser, T. E.; Reisner, E. *Nat. Energy*, **2017**, *2*, 17021.

9.4. Beyond water splitting

ARTICLES
https://doi.org/10.1038/s41557-019-0344-4
nature chemistry

Regio- and diastereoselective intermolecular [2+2] cycloadditions photocatalysed by quantum dots

Yishu Jiang[1], Chen Wang[2], Cameron R. Rogers[1], Mohamad S. Kodaimati[1] and Emily A. Weiss[1*]

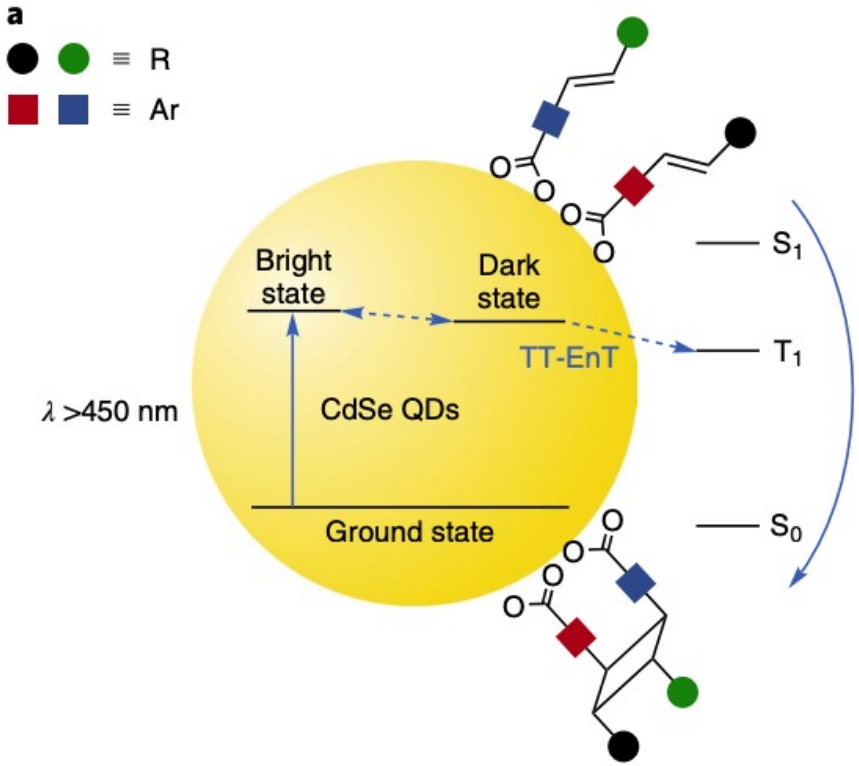

9.4. Beyond water splitting

JACS
JOURNAL OF THE AMERICAN CHEMICAL SOCIETY
pubs.acs.org/JACS
Article

Quantum Dot-Sensitized Photoreduction of CO_2 in Water with Turnover Number > 80,000

Francesca Arcudi,[¶] Luka Đorđević,[¶] Benjamin Nagasing, Samuel I. Stupp, and Emily A. Weiss*

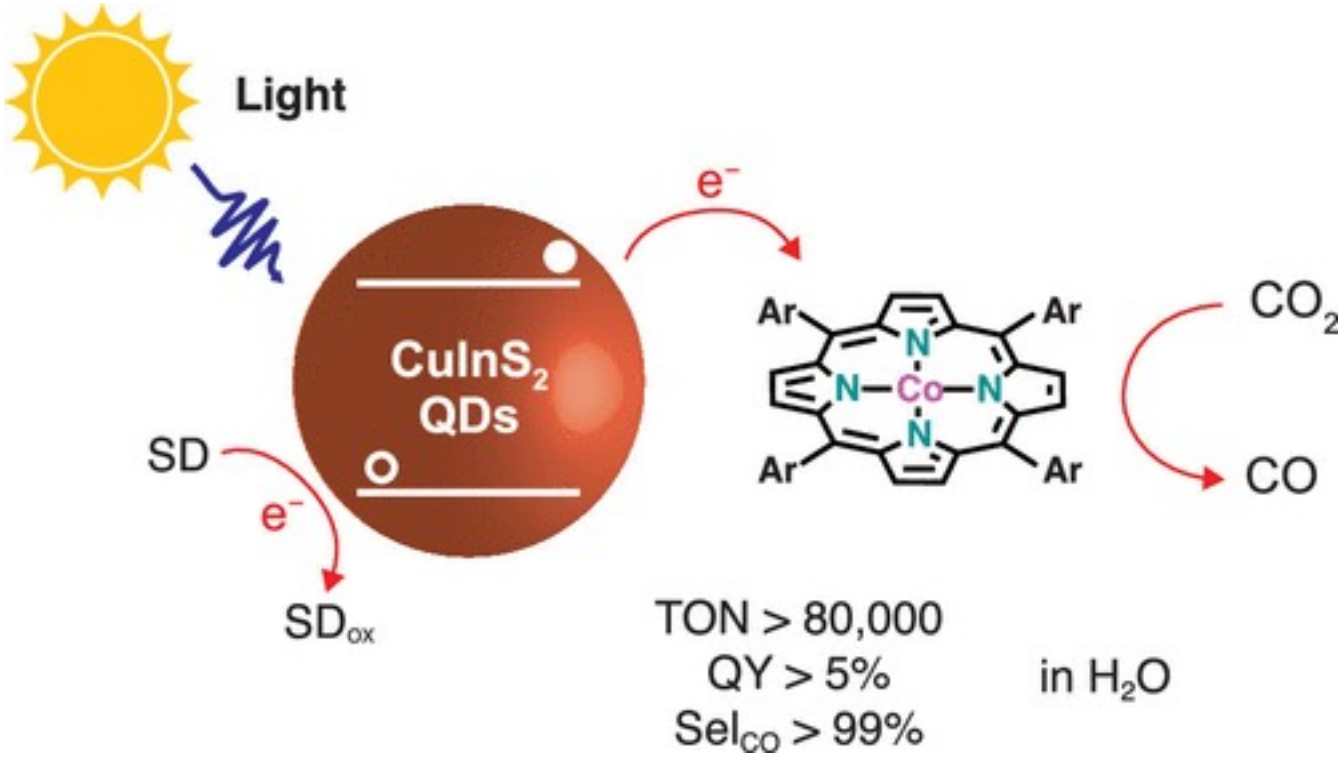

FINAL remarks:

Daniel Nocera

“The Sustainocene: era of personalized energy”